

# CHALMERS



## The Effect of Start/Stop Strategy on PEM Fuel Cell Degradation Characteristics

*Master of Science Thesis in the Master Degree Program Applied Physics*

ERIK ZAKRISSON

Department of Applied Physics

*Division of Condensed Matter Physics*

CHALMERS UNIVERSITY OF TECHNOLOGY

Gothenburg, Sweden, 2011



# The Effect of Start/Stop Strategy on PEM Fuel Cell Degradation Characteristics

*Master of Science Thesis in the Master Degree Program Applied Physics*

ERIK ZAKRISSON

Department of Applied Physics  
*Division of Condensed Matter Physics*  
CHALMERS UNIVERSITY OF TECHNOLOGY  
Gothenburg, Sweden, 2011

# The Effect of Start/Stop Strategy on PEM Fuel Cell Degradation Characteristics

*Master of Science Thesis in the Master Degree Program Applied Physics*

Erik Zakrisson

©ERIK ZAKRISSON, 2011, all rights reserved

Department of Applied Physics  
Division of Condensed Matter Physics  
CHALMERS UNIVERSITY OF TECHNOLOGY  
SE-412 96 Gothenburg  
Sweden  
Telephone +46 (0) 31-772 1000  
Department of Applied Physics, Gothenburg, 2011

# The Effect of Start/Stop Strategy on PEM Fuel Cell Degradation Characteristics

ERIK ZAKRISSON

Department of Applied Physics  
Division of Condensed Matter Physics  
Chalmers University of Technology

## Abstract

Fuel cells hold the ability to fulfill the objectives of an energy production that is effective, virtually free from green house gas emissions and independent from locally existing raw materials. The most promising type of fuel cell for lightweight vehicles and small scale energy production is the PEM fuel cell, due to its short start-up times and low operating temperatures. The development in the last decade has enabled satisfying power limits of the PEM fuel cell, which has resulted in an aim to reduce the price and receive a prolonged durability. Conditions during start and stop events result in a severe degradation of the fuel cell, which makes strategies to mitigate the impact important.

Two protective strategies have been developed and evaluated, one for start-up and one for shutdown. The strategy tests were performed in laboratory where the fuel cells were subjected to repetitive start/stop cycles. The performance reduction was measured at  $0.5 \text{ A/cm}^2$  for each cycle and the degradation was analysed with electrochemical *in situ* methods.

The start-up strategy resulted in a potential loss, at  $0.5 \text{ A/cm}^2$ , of  $69.7 \mu\text{V/cycle}$ . The corresponding potential loss for the shutdown strategy was  $92.5 \mu\text{V/cycle}$ . The degradation analysis showed that the electrochemically active platinum surface area was reduced after the preformed cycles, for both of the strategies.

**Keywords:** *PEM Fuel Cell, Degradation, Start-up, Shutdown, Carbon Corrosion, Reformate*

## Acknowledgments

This Master's Thesis is a collaborative work between the industrial sector and the academia. The project has given me great experiences and a lot of knowledge about several dimensions of the fuel cell technology.

I would like to express my gratitudes to my supervisors Patrik Johansson at Chalmers University of Technology and Andreas Bodén at PowerCell Sweden AB for enabling the project and for their support along the process. Matthew Iivity and Axel Baumann Ofstad at PowerCell Sweden AB have also assisted and guided me through different situations. I would especially like to thank Alejandro Oyarce at the Royal Institute of Technology for his assistance and everlasting interest during my laborative work in Stockholm.

Last but not least I would like to thank my family and friends for supporting and encouraging me during this project.

# Table of Contents

ABSTRACT .....	iii
ACKNOWLEDGMENTS .....	iv
TABLE OF CONTENTS .....	v
LIST OF FIGURES .....	vii
LIST OF TABLES .....	viii
LIST OF ABBREVIATIONS .....	ix
<b>Chapter 1:      <i>Introduction and Basic Theory</i></b>	<b>1</b>
1.1 ABOUT THIS THESIS .....	1
1.1.1 Limitations .....	1
1.2 INTRODUCTION .....	2
1.3 FUEL CELL THEORY .....	3
1.3.1 Construction and Function of the Fuel Cell Parts .....	4
1.3.2 Reasons for Degradation in Fuel Cells .....	6
1.3.3 Studies of Protective Start-up and Shutdown Strategies	10
1.4 METHODS FOR ANALYSING FUEL CELL DEGRADATION ....	11
1.4.1 Polarization Curve .....	12
1.4.2 Cyclic Voltammetry .....	16
1.4.3 Hydrogen Crossover Measurement .....	18
1.4.4 Impedance Spectroscopy .....	18

<b>Chapter 2:</b>	<b><i>Methods</i></b>	<b>23</b>
2.1	CHOSEN TESTS FOR REDUCING FUEL CELL DEGRADATION	23
2.1.1	Start-up Strategy with Voltage Control .....	24
2.1.2	Recirculation of Hydrogen Before Shutdown .....	25
2.2	LABORATORY EQUIPMENT .....	26
2.3	PERFORMED ANALYSIS METHODS .....	28
<b>Chapter 3:</b>	<b><i>Results and Discussion</i></b>	<b>31</b>
3.1	START-UP STRATEGY .....	31
3.2	SHUTDOWN STRATEGY .....	33
3.3	ANALYSIS OF THE DEGRADATION .....	34
<b>Chapter 4:</b>	<b><i>Conclusion and Future Work</i></b>	<b>43</b>
<b>Bibliography</b>		<b>45</b>

# List of Figures

1.1	Cost and durability targets for automotive fuel cell systems...	2
1.2	Simple schematic of a PEM fuel cell .....	4
1.3	Cross-section of a cathode electrode .....	5
1.4	Electrolyte potential during reverse current conditions.....	7
1.5	Example of a polarization curve and a Tafel plot .....	13
1.6	A typical result of cyclic voltammetry for a fuel cell cathode..	17
1.7	Typical hydrogen crossover current measurement.....	19
1.8	Equivalent circuit and its related Nyquist plots.....	21
2.1	Typical voltage and current curves for two cycles of the start-up strategy .....	25
2.2	Voltage and current profiles for two cycles of the recycling shutdown strategy .....	26
2.3	Schematic of the experimental setup.....	27
3.1	Measurement of OCV and performance during the start-up strategy .....	32
3.2	OCV and performance during the recirculation strategy .....	33
3.3	Polarization curves of initial measurements and after cycling with each strategy .....	35
3.4	Tafel plot for the performed measurements .....	36
3.5	Comparison of the increase of each loss in the polarization curve	37
3.6	Partial pressure sweep before and after the cycling.....	38
3.7	Impedance spectroscopy performed at low current density.....	39
3.8	Impedance spectroscopy performed at high current density....	40
3.9	Results of the cyclic voltammetry measurements before and after operating strategy cycling .....	41
3.10	Hydrogen crossover measurements for the strategies .....	42

# List of Tables

2.1	Algorithm for the start-up strategy .....	25
2.2	Algorithm for the recirculation shutdown strategy .....	26
2.3	Parameters for the different analysis methods .....	30
3.1	Comparison of the degradation parameters .....	42

# List of Abbreviations

- AC** Alternating Current
- APU** Auxiliary Power Unit
- CPE** Constant Phase Element
- CV** Cyclic Voltammetry
- ECSA** ElectroChemical platinum Surface Area
- GDL** Gas Diffusion Layer
- HOR** Hydrogen Oxidation Reaction
- KTH** Royal Institute of Technology
- MEA** Membrane Electrode Assembly
- MPL** MicroPorous Layer
- MSL** Macroporous Substrate Layer
- OCV** Open Circuit Voltage
- ORR** Oxygen Reduction Reaction
- PEM** Polymer Electrolyte Membrane
- PTFE** Polytetrafluoroethylene
- RHE** Reversible Hydrogen Electrode



# Chapter 1

## Introduction and Basic Theory

### 1.1 About this Thesis

This project is a collaboration between PowerCell Sweden AB, Chalmers University of Technology and the Royal Institute of Technology (KTH). The practical laborations on single cells were performed at KTH on fuel cell materials from PowerCell. The Master's Thesis examination was performed by Chalmers.

#### 1.1.1 Limitations

This Master's Thesis was only focused on the Polymer Electrolyte Membrane (PEM) fuel cell, other types of fuel cells were not regarded. This means that when fuel cells are mentioned in the following report it is the PEM fuel cell that is referred, if nothing else is specified.

There are many different reasons for degradation of fuel cells. However the tests in this thesis were only aimed to analyse the degradation induced by start and stop events. The only part of the fuel cell that was regarded in this project was the Membrane Electrode Assembly (MEA), that is the anode, cathode and membrane. Degradation is more or less present on all parts of the fuel cell, but these were not investigated and are not discussed further in this report. The only performed measurements to evaluate the degradation was *in situ* methods.

## 1.2 Introduction

Increasing concerns about climate change and aims to develop a sustainable society have resulted in several restrictions and regulations regarding energy efficiency and emissions of green house gases. Fuel cells hold the potential to fulfill these objectives, due to their low emissions, high efficiency and the ability to be fueled with energy produced with renewable sources such as wind, solar or biomass. The fact that the fuel can be produced anywhere states a promising step toward a desired energy security in the world. One of the areas where fuel cells are applicable is in the automotive industries. For lightweight vehicles, the PEM fuel cell is a promising type of cell due to low operating temperature and short start-up time (Borup et al., 2007).

Recent development has enabled a satisfying level in power from the fuel cell, but there still remain challenges for a large scale and commercial use of fuel cells. The two main concerns are the interlinked issues of cost and durability of the fuel cells (de Bruijn et al., 2008). Figure 1.1 shows the present and projected targets for the cost and durability for fuel cells in the automotive sector, established by the U.S. Department of Energy (2009). To be able to reach these targets, new materials and operation strategies have to be developed.

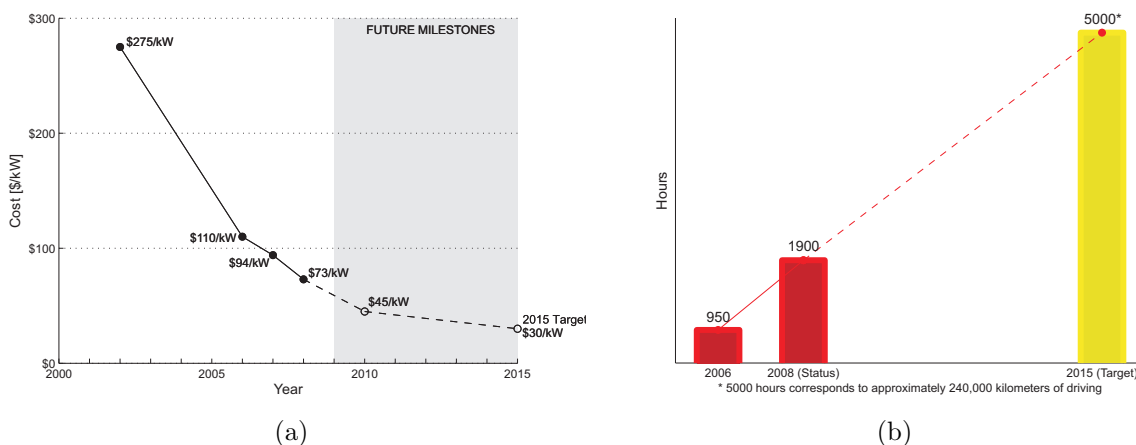


**Figure 1.1:** Targets for cost, projected to a high-volume manufacturing (a), and durability under real-world conditions (b) for automotive fuel cell systems. The data is apprehended from U.S. Department of Energy (2009).



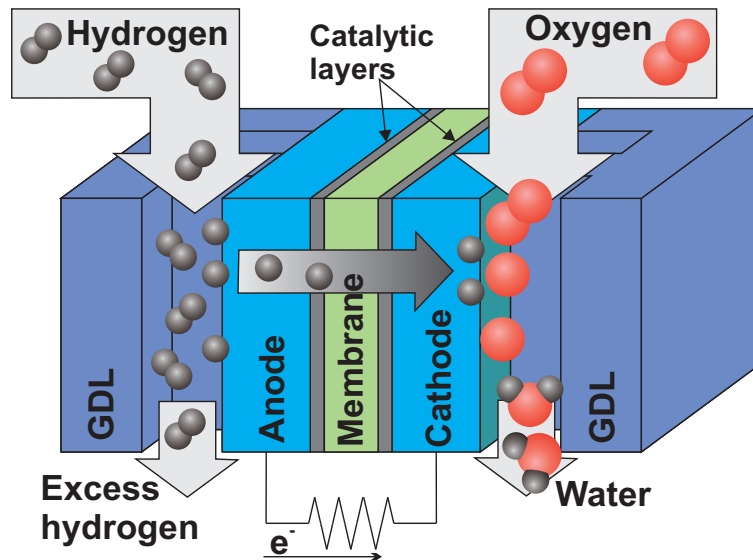


**Figure 1.2:** Simple schematic of a PEM fuel cell fueled with hydrogen gas at the anode and oxygen at the cathode.

Individual fuel cells are performing at approximately 0.7 V at a current density of 1 A/cm<sup>2</sup>, which is not useful for most real world applications. By connecting several single cells in series a fuel cell stack is built. The power in a fuel cell stack can be modified to fit any possible use, by changing the number of single cells in it and the active area of the fuel cell. The power from a fuel cell stack with  $n = 100$  single cells with an area of  $A = 100$  cm<sup>2</sup>, is calculated in equation 1.2.

$$P = UI = n \cdot u \cdot A \cdot i = 100 \cdot 0.7 \cdot 100 \cdot 1 = 7 \text{ kW} \quad (1.2)$$

### 1.3.1 Construction and Function of the Fuel Cell Parts

One of the most common polymer electrolyte membranes is Nafion<sup>®</sup>, that consist of a polymeric material base of carbon and fluorine atoms, called Polytetrafluoroethylene (PTFE), and is commonly used in Teflon<sup>®</sup>. The PTFE is resistant to chemical attacks and it is a strong polymer, a property needed to produce thin membranes. PTFE is hydrophobic, which is an important feature to drive the produced water out from the membrane,

thus preventing flooding. A side chain with an acidic sulfonic end-group is attached to the basic PTFE. The most important feature of the sulfonic acid ( $\text{HSO}_3$ ) is that it is hydrophilic. This means that hydrophilic regions are created in the otherwise hydrophobic structure of the membrane, in which protons are weakly bound. The result is that the protons can move quite easily in a well hydrated membrane, where the hydrophilic regions are large (Larminie & Dicks, 2003). The electrodes are attached on each side of the membrane, which completes the MEA.

The electrocatalytic layer is placed on the MEA or on the GDL, as shown in figure 1.3, and is often constructed of platinum (Pt) particles supported on electron conductive carbon particles, and a proton conducting ionomer (Young et al., 2009). The catalytic platinum particles allow reactions on their surface, which lower the activation energy for the reactions, resulting in an increased reaction rate. Platinum is expensive and contributes to a large extent to the high price of PEM fuel cells, which makes it desirable to use the platinum as effective as possible. This fact results in small particles supported in a way to maximise the active surface area of the platinum particles (Larminie & Dicks, 2003).

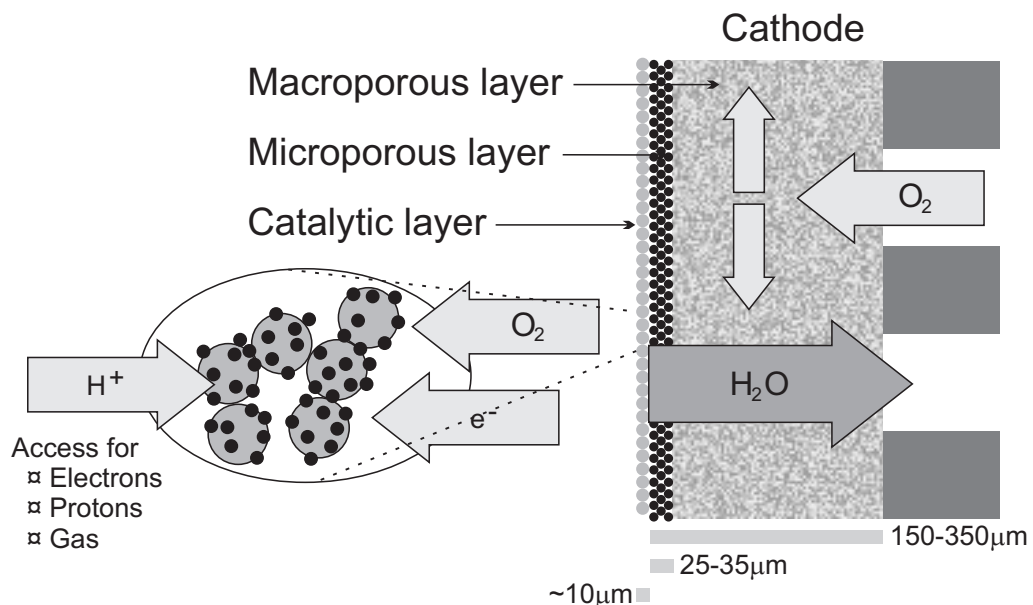


**Figure 1.3:** Cross-section of a cathode electrode. Pathways for gas, protons and electrons are shown, as well as an illustration of the catalytic particles. The figure is re-drawn with inspiration from de Bruijn et al. (2008).

The GDLs are constructed of one Macroporous Substrate Layer (MSL), and one thin MicroPorous Layer (MPL), as the schematical cross-section of a cathode electrode in figure 1.3 illustrates. The GDLs lets the gas through and distributes it equally over the catalytic layer, they also conduct electrical current and provide paths for guiding the produced liquid water from the MEA to the flow channel. The macroporous layer is made of a carbon fiber matrix with a high rate of voids. The microporous layer is a hydrophobic structure made by a mixture of a carbon powder, called carbon black, and fluoropolymer (Borup et al., 2007).

### 1.3.2 Reasons for Degradation in Fuel Cells

There are numerous reasons for a fuel cell to degrade when it is active in an automotive application. This section will enlighten important sources for degradation that are present in start-up and shutdown sequences. Other reasons for degradation, discussed by Borup et al. (2007), are for example impurities in the gases, such as CO or NH<sub>3</sub> in the fuel, and SO<sub>x</sub>, NO<sub>x</sub> or particulates in the air. Depending on the type of impurity, it is possible that the contaminants can adsorb onto the electrocatalytic surfaces and reduce the active area, changing proton conduction in the ionomer or having an impact on water and/or gas transport in the gas diffusion layers. The fuel cell can also be degraded due to subfreezing temperatures in the surroundings, which causes ice formation of the water inside, that mechanically damages the fuel cell (Borup et al., 2007).

#### Start/stop Cycling and the Reverse Current Mechanism

When the fuel cell is inactive, air is diffusing into the anode side through the membrane or via not perfectly working seals and gas connections. This causes a fuel/air front when the fuel is turned on. During investigation of the situation of a fuel/air front, it is convenient to separate the fuel cell into two different regions, one fueled with hydrogen and one fueled with oxygen, as illustrated in the top of figure 1.4. Reiser et al. (2005) investigated this reverse current mechanism and found out the following: Before introduction of hydrogen, both the anode and cathode electrode potentials ( $V_m^a$  and  $V_m^c$ ) are close to the equilibrium potential of the oxygen

$(V_{O_2}^{eq} \approx 1.23 \text{ V})$ , with respect to the electrolyte potential ( $\Phi$ ), resulting in a cell potential close to 0 V ( $V_{cell} = V_m^c - V_m^a$ ). As soon as the hydrogen is introduced into region A of the anode (see figure 1.4), it oxidizes and  $V_m^a$  is changed to a value of the equilibrium potential of hydrogen ( $V_{H_2}^{eq} \approx 0.0 \text{ V}$ ), compared to  $\Phi$ , which raises  $V_{cell}$  to about 0.85 V. The potential in the interface of the electrode and electrolyte ( $V_m^a - \Phi$ ) has to be maintained at  $V_{O_2}^{eq}$ , which implies that  $\Phi$  decreases, since the high electron conductivity of the anode electrode keeps  $V_m^a$  constant. Because of the lowering of  $\Phi$ , and that  $V_m^c$  is constant due to high electron conductivity, the interfacial potential  $V_m^c - \Phi$  becomes about 1.44 V, which is larger than  $V_{O_2}^{eq}$ . The high interfacial potential is thereby high enough to allow carbon corrosion of the catalyst supports. The estimated electrolyte potential curve in the different regions is shown in figure 1.4.

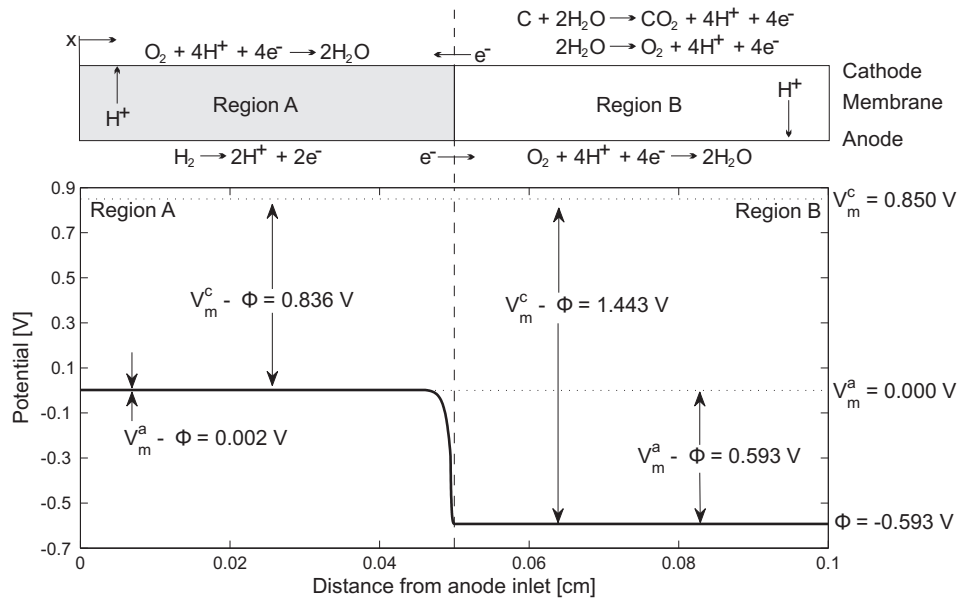


**Figure 1.4:** Electrolyte potential along the anode flow path during conditions that gives reverse current. The fuel/air front is marked as a dashed line in the middle of the flow path ( $x = 0.05$ ). The schematic in the top of the image illustrates the two regions and the reactions occurring in each region. Re-drawn from Reiser et al. (2005).

The high interfacial potential difference at the cathode causes oxygen evolution and carbon corrosion, that damages the catalyst supportive structures. The protons released from the water and carbon reactions at the cathode side in region B are diffusing from the cathode to the anode, due to a shorter pathway in the vertical direction (de Bruijn et al., 2008). At

the anode side the protons are consumed in the Oxygen Reduction Reaction (ORR), which results in a reverse current mechanism.

The phenomenon of reverse current also appears when there is fuel starvation in some parts of the fuel cell. Fuel starvation is a problem in fuel cells stacks, due to difficulties to maintain an even gas distribution to all the cells in the stack. Using gas mixtures, such as reformat as fuel, also increase the risk for fuel starvation (Baumgartner et al., 2006). Even if there are shortages of hydrogen in some regions of the anode, the electrode potential is kept constant due to the high conductivity, which can lead to high cell potential differences (de Bruijn et al., 2008).

### Temperature and Humidity

The life time of a fuel cell is maximised if the cell can be operated at constant temperature and with well hydrated gases. These parameters can be controlled when the fuel cell is operated at constant intermediate currents. In an application with dynamic loads, however, temperature and humidity are affected by the current taken from the fuel cell when the stoichiometric ratios are fixed. Operation at low currents results in a relatively wet and cold cell, while operation at higher currents increases the temperature, resulting in a more dry cell membrane. The ionomers in the membrane swells with water uptake, which implies compressive mechanical stresses in the membrane at high relative humidities, and tensile stresses during drier operation respectively. The combination of loss in ductility and the extreme stresses on the MEA can lead to a mechanical failure (Borup et al., 2007).

Except the durability issue, due to humidity and temperature, the performance is also affected. Nakamura et al. (2009) showed that a fuel cell operating at low humidity conditions increased the ohmic losses and the mass transport losses. That the ohmic losses are reduced relates to the fact that the ionic conduction in the membrane increases with higher water content. The mass transport at the cathode side is slightly blocked by water at high humidities, but at low humidities the oxygen transport is reduced over the catalytic layer, which increases the mass transport losses (Nakamura et al., 2009). Ohmic losses and mass transport losses will be

further explained in section 1.4.1. The humidity can also have an impact on the active area of the platinum catalysts at the cathode side. Kim et al. (2010a) showed that start/stop cycling at different relative humidities at the cathode, and constant relative humidity at the anode, resulted in increased degradation at higher humidities. The reason for the increased degradation was shown to be linked to increased charge transfer resistance ( $R_{ct}$ ) and a loss of electrochemically active area. Kim et al. (2010b) clearly showed that the increased humidity allowed a higher reaction rate, that caused carbon corrosion and platinum agglomeration, oxidation, dissolution and/or migration, which in turn implied a higher  $R_{ct}$  and a loss of active area. Carbon corrosion is discussed further later in this section.

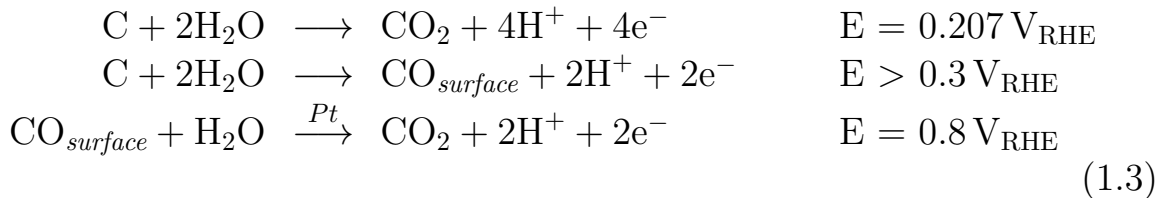
### Dynamic Cell Potentials

A fuel cell during operation in an automotive application is exposed to dynamic variations in cell potential, as various loads are applied. Several properties of the electrode materials are linked to the potential, such as the hydrophobicity of the surfaces and the oxide coverage of the carbon and the platinum particles (Borup et al., 2007). Experimental data indicates that the electrochemically active area reduces rapidly, which is a result of platinum dissolution caused by potential cycling (Borup et al., 2007). This effect has also been modeled by Darling & Meyers (2003), who found that platinum is stable at both high and low potentials, but that a rapid dissolution occurs when transitioning from low to high potentials. Gasteiger et al. (2008) discuss that the potential variations are largest at the cathode electrode, caused by slower kinetics of the ORR, while the faster kinetics of the Hydrogen Oxidation Reaction (HOR) keeps the anode electrode potential almost constant. Yu et al. (2009) concluded that potential cycling can cause carbon corrosion and can be assigned to be about 8% of the total carbon loss.

### Carbon Corrosion

Carbon is oxidized, or corroded, to carbon dioxide ( $\text{CO}_2$ ) at relatively low potentials, as described in the reactions in equation 1.3 (de Bruijn et al., 2008), where  $V_{\text{RHE}}$  denotes the potential difference versus the Reversible

Hydrogen Electrode (RHE). The RHE is used as reference since it is stable at 0 V in fuel cells. The kinetics in the carbon reactions is however quite slow, which means that the carbon is stable at normal operating conditions with potentials between 0–1 V<sub>RHE</sub> of a PEM fuel cell (Young et al., 2009). As mentioned in previous sections, potential increase occurs during start-up or shutdown sequences, fuel starvation or reverse current situations. These elevated potentials can result in a cathode potential larger than 1.0 V<sub>RHE</sub>, which increases the reaction rates and causes a significant carbon corrosion (Meyers & Darling (2006); Yu et al. (2009)).



Carbon corrosion is responsible for a large part of the degradation of the fuel cell performance. As the carbon oxidizes, the support for the platinum particles disappear, leaving the platinum free to agglomerate, oxidize or dissolve, which reduces the electrocatalytic active area. Yu et al. (2009) showed, during corrosion cycles, a thinning of the cathode catalytic layer from about 15 μm to 5 μm, while the membrane and anode catalytic layer thickness remained unchanged. This results in large potential losses at higher current densities. de Bruijn et al. (2008) discuss that the carbon corrosion also has an effect on the GDL and MPL of the cathode. The corrosion changes the porous structures and the MPL gets more hydrophilic. The degradation of the GDL affects the water and gas management at the cathode side, which increase the potential losses due to mass transport.

### 1.3.3 Studies of Protective Start-up and Shutdown Strategies

Until some 5–10 years ago, the most important question in the fuel cell technology was to improve the specifications for power density (de Bruijn et al., 2008). This indicates that most of the work made to improve the durability of fuel cells in different environments has occurred quite recently.

Shen et al. (2009) developed a start-up strategy where the anode is purged with nitrogen prior an introduction of the hydrogen fuel. This strategy resulted in low potential difference between the cathode and the anode, which implies lower carbon corrosion. It was also found that if a fuel/air boundary can not be avoided, an introduction of fuel at a higher flow rate was preferable. The higher flow rate still results in a high potential difference, but during a shorter time, which reduces the carbon corrosion. Another tested start-up strategy is to apply a dummy load as long as the fuel fills the anode compartment (Kim et al. (2009); Perry et al. (2006); Shen et al. (2009)). The dummy load lowers the potential difference and carbon corrosion is thereby avoided. This type of voltage control reduced the degradation from  $\sim 100 \mu\text{V}/\text{cycle}$  to  $\sim 4 \mu\text{V}/\text{cycle}$  in a test made by Perry et al. (2006). A third strategy has been tested by Jo et al. (2010), where the hydrogen is supplied to the anode prior to the introduction of oxygen on the cathode side. This strategy resulted in decreased power loss and a reduced electrochemically active catalyst surface area loss.

Shutdown strategies have also been developed to improve the durability of fuel cells. Kim et al. (2009) tested a nitrogen purge strategy on the anode, that lowered the potential difference at shutdown and reduced degradation of the MEA. Ofstad et al. (2008) tried to purge the anode with air at the shutdown sequence and found that a higher flow rate reduced the carbon corrosion. Dummy load strategies where the remaining hydrogen is consumed before shutdown have been developed as well (Shen et al. (2009); Perry et al. (2006)). The dummy load reduces the cell potential which limits the carbon corrosion. A Master's thesis made by Ivity (2010) showed that an air purge shutdown strategy can be as good as a load purge. The degradation after 1200 cycles for these strategies was only a few  $\mu\text{A}/\text{cm}^2$  per cycle. This result was compared to a scenario where no strategy was implemented, which showed a severe degradation after only 200 cycles.

## 1.4 Methods for Analysing Fuel Cell Degradation

The methods used in order to analyse the degradation of a fuel cell are electrochemical *in situ* methods. It is also possible to use *ex situ* measurements, such as measuring the amount of different species in the exhaust

gas mixture to get a direct indication of carbon corrosion, or actually see the physical degradation of the MEA or GDLs in an electron microscopy technique. The size of the platinum particles is possible to measure with X-Ray diffraction. The electrochemical *in situ* measurement techniques are however much more easy to perform and all that is needed is a potentiostat to control and measure the current and the potential. Furthermore, it is easy to relate the data to real fuel cell performance. This section will describe the electrochemical *in situ* measurements.

### 1.4.1 Polarization Curve

When using a polarization curve measurement it is possible to extract a lot of information of different fuel cell phenomena. This section will first describe the basics, then different degradation measures.

The characteristic appearance of a fuel cell's polarization curve can be seen in figure 1.5(a). The polarization curve has three different regions, which is a result of four major irreversible potential losses. Two of the losses can not be separated in the polarization curve and are combined into a total region of activation losses. The polarization curve can be modeled with equation 1.4 (Gasteiger et al., 2004), where the resulting voltage is a subtraction of each loss from the thermodynamically reversible potential ( $E_{rev}$ ). The losses in equation 1.4 are due to internal currents and fuel crossover ( $\eta_{i_x}$ ), resistance in all parts of the fuel cell ( $iR_{\Omega}$ ), losses for the HOR and the ORR,  $\eta_{HOR}$  and  $\eta_{ORR}$  respectively, and losses due to transport of gases ( $\eta_{tx}$ ).

$$E_{cell}(i) = E_{rev}(p_{H_2}, p_{O_2}, T) - iR_{\Omega} - \eta_{i_x} - \eta_{HOR}(i) - \eta_{ORR}(i) - \eta_{tx}(i) \quad (1.4)$$

The thermodynamic reversible potential can be calculated with equation 1.5, where  $\Delta g_f$  is the difference in Gibb's free energy of formation per mole, that is the energy gained when two reactants form a product (Larminie & Dicks, 2003). One example is the change in energy when hydrogen and oxygen react to form water as a product. The minus sign in equation 1.5 comes from the convention that when energy is gained in a reaction,

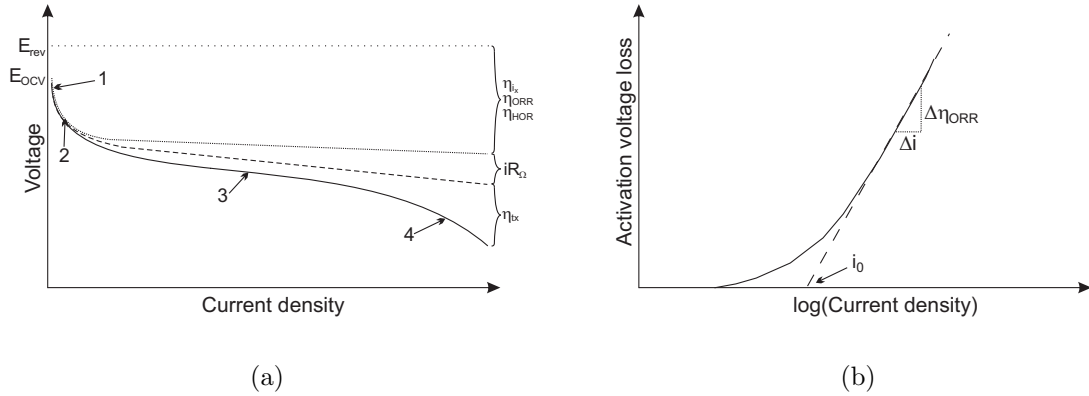


**Figure 1.5:** (a) Example of a polarization curve for a fuel cell. The four irreversible losses are numbered, the dashed and dotted lines are different corrections to improve the analysis. (b) A typical Tafel plot for a fuel cell. The dashed line is a non-linear logarithmic fit of the linear region of the measured curve. The exchange current density  $i_0$  is marked and  $A$  is the slope of the fitted line.

the Gibb's free energy is negative (Larminie & Dicks, 2003). Gibb's free energy is temperature and pressure dependent, hence also the  $E_{rev}$  have these dependences.

$$E_{rev} = -\frac{\Delta g_f}{zF} = -\frac{g_f^{products} - g_f^{reactants}}{zF} \quad (1.5)$$

The constants  $z$  and  $F$  in equation 1.5 are the number of electrons released in the HOR and Faraday's constant respectively. The  $E_{rev}$  for a hydrogen fuel cell operating at  $80^\circ\text{C}$ , forming water in the gas phase, can be calculated as in equation 1.6.

$$E_{rev} = -\frac{\Delta g_f}{zF} = -\frac{-226.1 \cdot 10^3}{2 \cdot 96485} \approx 1.2 \text{ V} \quad (1.6)$$

To get a more qualitative understanding of the impact from each loss in an experiment, it is possible to measure the ohmic resistance ( $R_\Omega$ ) at each current and receive a resistance corrected cell voltage  $E_{iR-corr} = E_{cell} + iR_\Omega$ . A second correction of the polarization curve is to add the hydrogen crossover current to the measured current to get a corrected current density

( $i_{eff}$ ) as described in equation 1.7 (Gasteiger et al., 2004). One method to measure hydrogen crossover current is presented in section 1.4.3.

The following four characteristics can be accessed via polarization curves:

### 1. Fuel Crossover and Internal Currents, $\eta_{i_x}$

Although a fuel cell electrolyte is designed to conduct positive ions, some electrons pass through as well. Since these electrons are not conducted through the external circuit, they are not useful and give rise to internal currents. There is also an amount of fuel that diffuses from the anode through the electrolyte to the cathode, where it reacts directly with the oxygen without producing any current to the external circuit. The amount of wasted fuel is known as fuel crossover. The effect of internal currents and fuel crossover in PEM fuel cells is a small reduction in the useful current in the size of a few mA/cm<sup>2</sup>. By naming this current  $i_x$ , it is possible to make a correction of the current density as in equation 1.7. The Open Circuit Voltage (OCV) is the voltage when the fuel cell is idled and can be calculated by  $E_{OCV} = E_{rev} - \eta_{i_x}$ , where  $\eta_{i_x}$  is the voltage loss due to internal currents and fuel crossover (Yuan et al., 2010).

$$i_{eff} = i + i_x \quad (1.7)$$

The fuel crossover can be reduced by using thicker membranes, this will however reduce the ionic conductivity of the membrane.

### 2. Activation Losses, $\eta_{HOR}$ and $\eta_{ORR}$

Activation losses are caused by the fact that a proportion of the total voltage is needed in the kinetic of the HOR and ORR. A certain amount of voltage is also needed to transport the electrons to or from the electrodes, thus some of the useful energy is lost. This electron transport is referred to as the exchange current density ( $i_0$ ), which depends on temperature and gas pressure. The  $\eta_{ORR}$  and the  $\eta_{HOR}$  can be combined with the loss due to internal currents and fuel crossover. This total activation loss term can be described with the Tafel equation (1.8), where  $A$  is a material constant called the Tafel slope,  $i_{eff}$  is the corrected current density and  $i_0$  is the exchange current density for the ORR reaction (Jo et al., 2010). Gasteiger et al. (2004) found

that  $\eta_{HOR}$  is negligible in these types of experiments with hydrogen at the anode side, due to the fast kinetics in the HOR compared to the ORR, which is the reason that  $\eta_{HOR}$  is excluded from equation 1.8.

$$\eta_{ORR}(i) = A \log\left(\frac{i_{eff}}{i_0}\right) = A \log\left(\frac{i + i_x}{i_0}\right) \quad (1.8)$$

The constant  $A$  in equation 1.8 can be obtained from experimental data in the low current density region where the mass transport losses ( $\eta_{tx}$ ) are negligible. When plotting the  $iR$ -corrected potential against the logarithm of the corrected current density, the slope of the graph corresponds to  $A$ . By making a non-linear logarithmic fit of the linear region described above, the ORR exchange current can be achieved, where the fitted line crosses the x-axis. This is illustrated in figure 1.5(b).

To reduce the activation losses an increase in reaction rate is wanted. This can be achieved by increasing the temperature, use more effective catalysts, increasing the active surface of the catalysts, increasing the amount of reactant or increasing the pressure.

### 3. Ohmic Losses, $iR_\Omega$

Both the electrodes and the membrane, that conduct electrons and protons respectively, have a certain amount of resistance. The total ohmic resistance can be separated into three terms, as in equation 1.9, where  $R_{e^-}$  is the electronic resistance,  $R_{H^+,mem}$  is the protonic resistance in the membrane and  $R_{H^+,Ca}^{eff}$  is the effective protonic resistance in the cathode electrode (Carter et al., 2009).

$$R_\Omega = R_{e^-} + R_{H^+,mem} + R_{H^+,Ca}^{eff} \quad (1.9)$$

To reduce the ohmic losses it is important to use electrodes with high conductivity and to use thin membranes. There is, however, a trade-off as there are limitations of how thin the membrane can be without increasing fuel crossover, reducing the ability to support the electrodes or insulating the electrodes from each other and thereby prevent shortening.

#### 4. Mass Transport Losses, $\eta_{tx}$

At high current densities, the fuel and reactants are consumed faster than they are supplied, which can be seen as a characteristic voltage drop in the polarization curve. This effect can be expressed mathematically by describing the pressure drops at different current densities, but there are many problems when using this model, for example if air is used as oxidant instead of pure oxygen (Larminie & Dicks, 2003). The mass transport losses are also increased if the charge transfer resistance ( $R_{ct}$ ) is enlarged. The  $R_{ct}$  will be explained in section 1.4.4. The mass transport losses are certainly important when mixed gases are used as fuel and oxidant, instead of pure gases, for example reformer gas instead of  $H_2$  and air instead of  $O_2$ . To reduce the losses due to mass transport, it is important to keep the area around the electrodes clean from contaminants that will block the pathways. In PEM fuel cells it is thus important to have an effective transport of the produced water away from the cathode electrode.

A simple way to determine the amount of mass transport degradation at the cathode side, is by changing the partial pressure of oxygen when the fuel cell is under a constant load. This will give a faster reduction of potential as the amount of oxygen gas at the cathode side reduces. This potential loss is a result of more occupied pathways for the  $O_2$  molecules to the catalytic layer, when other gas molecules are blocking the way.

#### 1.4.2 Cyclic Voltammetry

Cyclic Voltammetry (CV) is a method to determine the ElectroChemical platinum Surface Area (ECSA) in fuel cells. Having hydrogen at the anode side and nitrogen at the cathode side and sweeping the potential, will result in a curve as in figure 1.6. In the potential sweep the anode can be used as reference electrode, since the electrode potential is close to zero due to the fast kinetics small currents of the HOR at the anode side (Marie et al., 2009).

The different numbers in figure 1.6 indicate different actions at the catalyst particles, which can be described as follows:

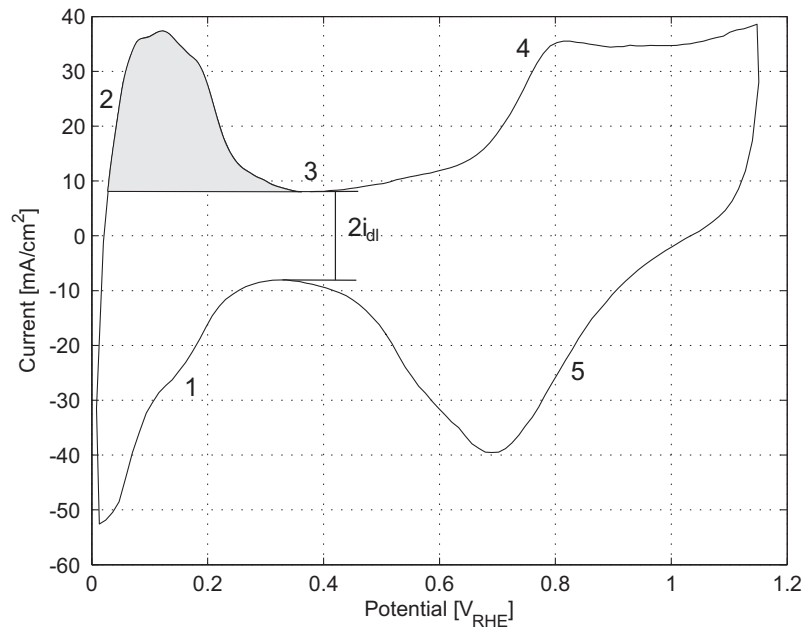


**Figure 1.6:** A typical result of a cyclic voltammetry for a fuel cell cathode. The shaded area is the ECSA of the cathode catalyst layer, the different numbers indicate the different actions on the catalyst layer.

1. Protons absorb to the Pt particles, and thereby creating a monolayer.
2. The potential is low and the hydrogen desorption from the Pt particles takes place.
3. At this point the platinum yields no specific current and the existing current is due to the double layer capacitance ( $C_{dl}$ ) via the relation in equation 1.10.
4. Due to the oxygen in the water inside the membrane, the Pt particles start to oxidize to PtO.
5. The PtO is reduced to Pt.

By calculating the area under the hydrogen desorption peak (shaded area in figure 1.6) the ECSA can be estimated (Lindström et al., 2010). A second value of great use that can be achieved from the CV is the double layer capacitance ( $C_{dl}$ ). The double layer is the area between the proton conducting membrane and the electron conducting electrode, whose capacitance can be calculated with equation 1.10, where the current  $i_{dl}$  is the

double layer current marked in figure 1.6 and  $dU/dt$  is the applied sweep rate during the CV (Marie et al., 2009).

$$i_{dl} = C_{dl} \frac{dU}{dt} \quad (1.10)$$

### 1.4.3 Hydrogen Crossover Measurement

The loss in potential due to fuel crossover and internal currents were introduced in section 1.4.1. The gas permeability constant ( $k_i$ ) of the membrane can be estimated with equation 1.11, where the index  $i$  is the specific gas,  $i_{i,x}$  is the crossover current,  $n$  and  $F$  are the valence and Faraday constant respectively,  $l$  is the thickness of the membrane and  $p_i$  is the gas pressure (Kocha et al., 2006). The gas permeation of a membrane is strongly dependent of the humidity and temperature, since the condition of the membrane is decided by the amount of water inside.

$$k_i = \frac{i_{i,x} l}{nF p_i} \quad (1.11)$$

The crossover current can be measured by introducing hydrogen as fuel at the anode and by using nitrogen gas at the anode. The cell potential is then scanned until the current response reaches a plateau, that implies that the crossover current is limited by the permeation rate of the membrane. Thus, at this point, the current is proportional to the gas pressure and the permeability coefficient, and inversely proportional to the thickness, according to equation 1.11. Figure 1.7 shows a typical crossover current response with a distinct plateau that starts around 0.1 V.

### 1.4.4 Impedance Spectroscopy

Impedance spectroscopy is a powerful tool to achieve information about the status of a fuel cell. By applying an Alternating Current (AC) with different frequencies it is possible to measure the impedance response. A fuel cell can be modeled as a more or less simple equivalent circuit, to which

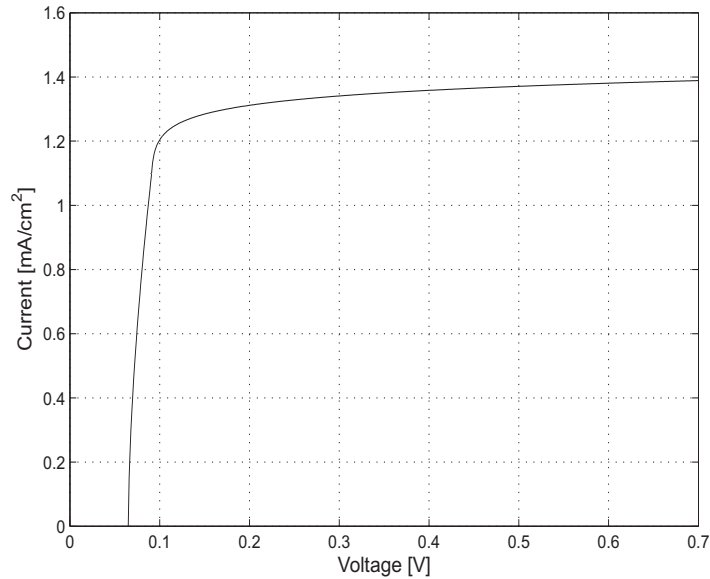


**Figure 1.7:** A typical hydrogen crossover current response. The current density starts to reach a plateau value around 0.1 V.

the measured data can be fitted. The most commonly used equivalent circuit is a resistance connected in series with a Constant Phase Element (CPE) in parallel with another resistance, as illustrated in figure 1.8(a) (Yuan et al., 2010). This circuit is a model of the membrane and the cathode, the anode can be modeled in a similar way, but the influence from the anode can, according to Yuan et al. (2010), be neglected due to the fast kinetics of the HOR. The impedance of a CPE is expressed in equation 1.13, where  $q$  is a constant of numerical values, the exponent  $n \in [-1, 1]$  describes the phase shift,  $\omega$  is the frequency and  $j$  the complex number<sup>1</sup> ( $j^2 = -1$ ). If  $n = -1, 0, 1$  the CPE is a pure inductance, resistance or a capacitance respectively, all other values in between are distortions of one of these elements. Figure 1.8(c) illustrates the impact on the impedance curve for different values of  $n$ . Equation 1.12 shows the impedance expression for a resistance and equations 1.14 and 1.15 show the sum of  $N$  impedance elements connected in series, or in parallel, respectively. The expression of the total impedance of the equivalent circuit in figure 1.8(a) is shown in equation 1.16.

<sup>1</sup> $j$  is chosen to represent the complex number instead of  $i$ , to avoid confusion with the current density.

$$Z_R = R \quad (1.12)$$

$$Z_{CPE} = q^{-1}(j\omega)^{-n} \quad (1.13)$$

$$Z_{Series}^{Tot} = Z_1 + Z_2 + \dots + Z_N \quad (1.14)$$

$$(Z_{Parallel}^{Tot})^{-1} = Z_1^{-1} + Z_2^{-1} + \dots + Z_N^{-1} \quad (1.15)$$

$$Z(\omega) = R_{mem} + [R_{ct}^{-1} + q\omega^n(\cos(\frac{\pi}{2}n) + jsin(\frac{\pi}{2}n))]^{-1} \quad (1.16)$$

The translation between the equivalent circuit and a real fuel cell is that  $R_{mem}$  is the resistance in the membrane, and the  $R_{ct}$  refers to the barrier that the electrons must pass between the electrode surface and the adsorbed species, or in the opposite direction. An increased  $R_{ct}$  is an indication of a worsened mass transport, since the effect on the potential decline is due to higher charge transfer resistance, and a reduced amount of adsorbed species, is similar (Young et al., 2010). The CPE is in this case an element representing the double layer capacitance  $C_{dl}$  between the membrane and the electrode, with a slight disturbance of the electrode. The disturbance can depend on a variety of properties, such as surface roughness, variations in electrode thickness or composition, a varied current distribution over the electrode or different reaction rates over the electrode surface (Yuan et al., 2010).

When plotting the imaginary part against the real part of the impedance, a Nyquist plot is gained. The Nyquist plot of the described equivalent circuit is a depressed semicircle, where  $n$  describes the deformation from an ideal semicircle. The left and right point where the curve crosses the real axis, is the high and low frequency regions of the impedance respectively, as marked in figure 1.8(b). At high frequencies, the total impedance is represented by the membrane resistance, which also can be seen from equation 1.16 where  $Z(\omega \rightarrow \infty) = R_{mem}$ . At low frequencies the impedance is a sum of the membrane and charge transfer resistances,  $Z(\omega \rightarrow 0) = R_{mem} + R_{ct}$  (Yuan et al., 2010).  $R_{ct}$  is thus obtained by determining the diameter of the semicircle.

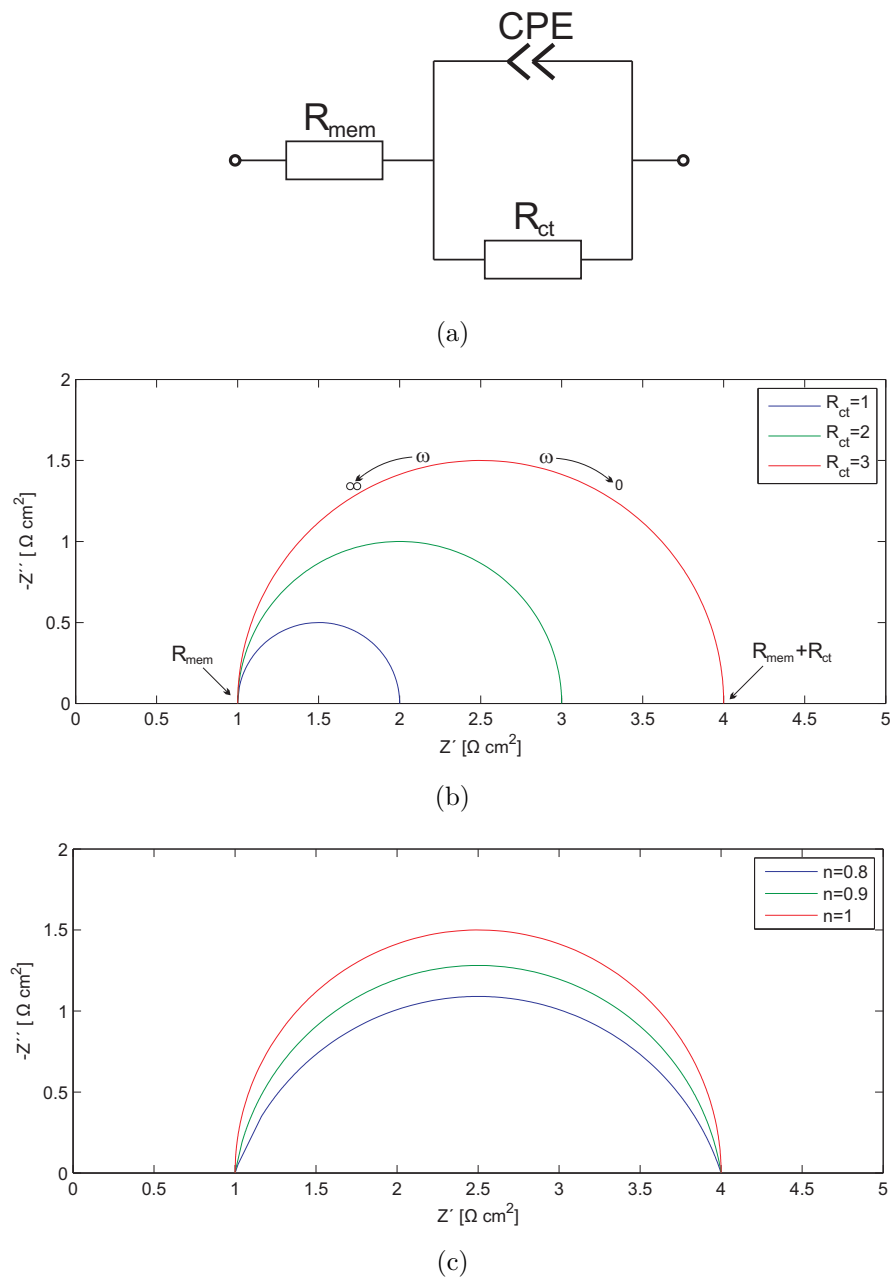


**Figure 1.8:** (a) An equivalent circuit of a fuel cell membrane and cathode. The circuit includes a membrane resistance  $R_{mem}$ , a charge transfer resistance  $R_{ct}$  and a CPE representing the double layer capacitance. (b) A Nyquist plot for different  $R_{ct}$ . The other parameters are  $q = 0.01 \Omega^{-1} s^{-1}$ ,  $n = 1$  and  $R_{mem} = 1 \Omega$  as marked in the image. (c) A Nyquist plot illustrating the function of the constant  $n$ , where  $R_{ct} = 3 \Omega$ ,  $R_{mem} = 1 \Omega$  and  $q = 0.01 \Omega^{-1} s^{-n}$ .



# Chapter 2

## Methods

The developed strategies and algorithms for analysing and minimising the fuel cell degradation are presented in this chapter. Experimental setups and equipment are also discussed.

### 2.1 Chosen Tests for Reducing Fuel Cell Degradation

A PEM fuel cell used in an automotive application is estimated to undergo over 30000 start/stop cycles during its lifetime (Kim et al., 2009). However, when different strategies to mitigate degradation due to start-up and shutdown are tested, less cycles are needed. For the strategies presented below, 1100 cycles were chosen to be enough to be able to evaluate the degradation.

The gas stoichiometries were chosen to prevent hydrogen and/or oxygen starvation when operating at  $1 \text{ A/cm}^2$ , which implies stoichiometry 2 at the cathode and 1.2 at the anode. The gas flows were then calculated via Faraday's law and the ideal gas law, as shown in equation 2.1, where  $\dot{V}_{gas}$  is the mass flow,  $I$  is the current where the chosen stoichiometry  $\lambda_{gas}$  is valid,  $R$  and  $T$  is the gas constant and temperature respectively. The remaining constants are the gas pressure  $P_{gas}$ , the Faraday constant  $F$ , the valence of the atoms  $z_{gas}$  and  $C_{gas}$ , which is the percentage of hydrogen or oxygen in the gas mixture introduced into the anode or cathode, respectively.

$$\begin{aligned}
n_{gas} &= \frac{It}{F \cdot z_{gas}} \\
V_{gas} &= \frac{n_{gas}RT}{P_{gas}} \\
\dot{V}_{gas} &= \frac{V_{gas}}{t} \\
\implies \dot{V}_{gas} &= \frac{IRT}{Fz_{gas}P_{gas}} \cdot \frac{\lambda_{gas}}{C_{gas}}
\end{aligned} \tag{2.1}$$

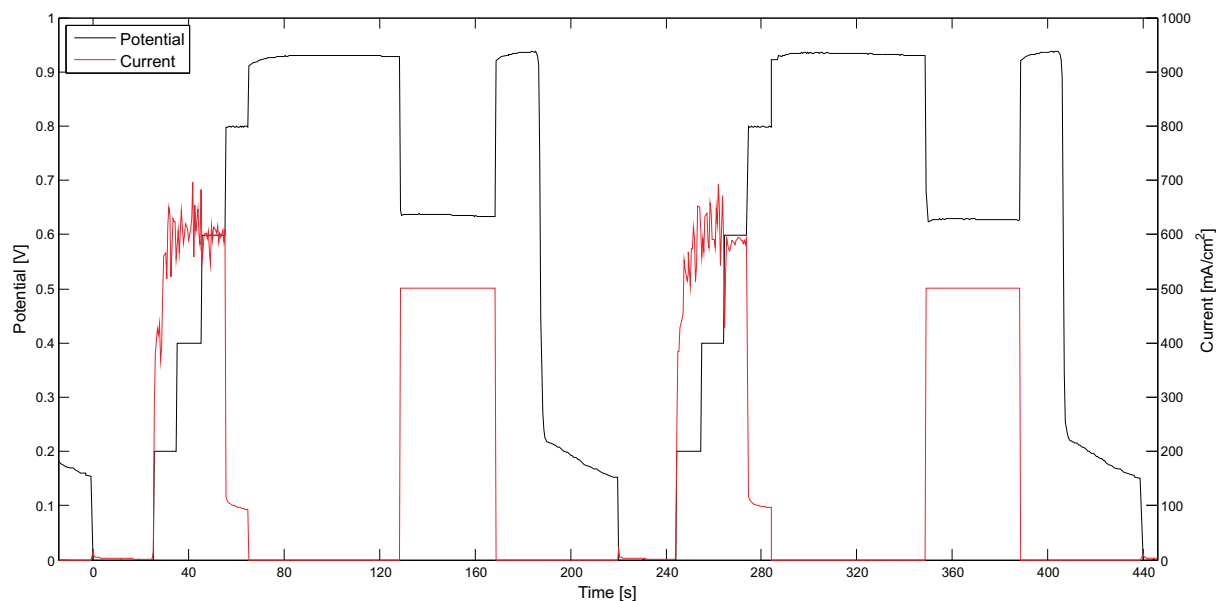
The fuel cell test stand used for the operation was designed at KTH which gave a circular single cell, with an area of 7 cm<sup>2</sup>. The MEA was pressurised with 3 bar and the cell temperature was kept at 70 °C. The relative humidity of the gases was controlled to 80 %. The reformat composition was 45 % H<sub>2</sub>, 32 % N<sub>2</sub> and 23 % CO<sub>2</sub>.

### 2.1.1 Start-up Strategy with Voltage Control

This strategy uses the fact that the fuel cell is driven by reformat. By consuming the hydrogen as it enters the fuel cell, the remaining gases in the reformat pushes the oxygen out from the anode, minimising the fuel/air boundary. To consume the hydrogen, a lower reformat flow was applied in the start-up sequence at the same time as the potential was controlled via the potentiostat. At first the potential was kept stable at 0 V until the fuel enters the anode, after that the potential was increased in steps of 0.2, 0.4, 0.6 and 0.8 V and kept for 10 s each, after the steps the potential was released to OCV. This strategy was chosen after testing different flow rates and different times at each potential step, while the cell temperature and current were measured to make sure that the hydrogen was consumed. An increased cell temperature could result in pin-holes in the membrane, due to local fuel starvation. The chosen parameters showed a low temperature increase, the hydrogen was consumed and the flow was relatively high to minimise the time of a fuel/air boundary. The shutdown of the fuel cell was an air purge of the anode. The algorithm is shown in table 2.1 and the corresponding current and voltage curves for two cycles are presented in figure 2.1.

**Table 2.1:** Algorithm for the start-up strategy.

Action	Time period
1. Purge the anode with dry air	30 s
2. Run the potential steps at lower flow rate	60 s
3. Run the fuel cell at OCV with full flow rate	40 s
4. Apply a load of $0.5 \text{ A/cm}^2$	40 s
5. Release the load and stay at OCV	20 s
6. Purge the anode with dry air	30 s
	Total: 220 s (3:40 min)

**Figure 2.1:** Typical voltage and current curves for two cycles of the start-up strategy.

### 2.1.2 Recirculation of Hydrogen Before Shutdown

When the excess hydrogen is recycled, all of it can be used in the cell. The hypothesis is that the hydrogen will be distributed over the whole cell, minimising local fuel starvation. By consuming all the hydrogen at the anode side, the only gases left will be nitrogen and carbon dioxide, hence the appearance of a fuel/air boundary as air diffuses into the anode compartment after shutdown is diminished. The algorithm for the recirculation cycles are shown in table 2.2. To consume the hydrogen a load program is applied after 80s. The load program algorithm is to apply currents of 20, 15, 10, 5 and  $1 \text{ mA/cm}^2$  until the voltage drops below 0.2 V. Between each consuming current, a waiting time of 35 s is applied, except between

the two last currents when the wait time is 5 s. The waiting times are sufficiently large to allow the remaining hydrogen to be recycled. Figure 2.2 shows typical current and voltage curves during two cycles.

**Table 2.2:** Algorithm for the recirculation shutdown strategy.

Action	Time period
1. Purge the anode with dry air	30 s
2. Fuel supply is turned on and the cell runs at OCV	10 s
3. Run the cell at 0.5 A/cm <sup>2</sup>	40 s
4. Start the pump if there is residual air in the recycling path	Last 5 s of step 3
5. Shut off fuel supply and run the load program	400 s
	Total: 480 s (8 min)

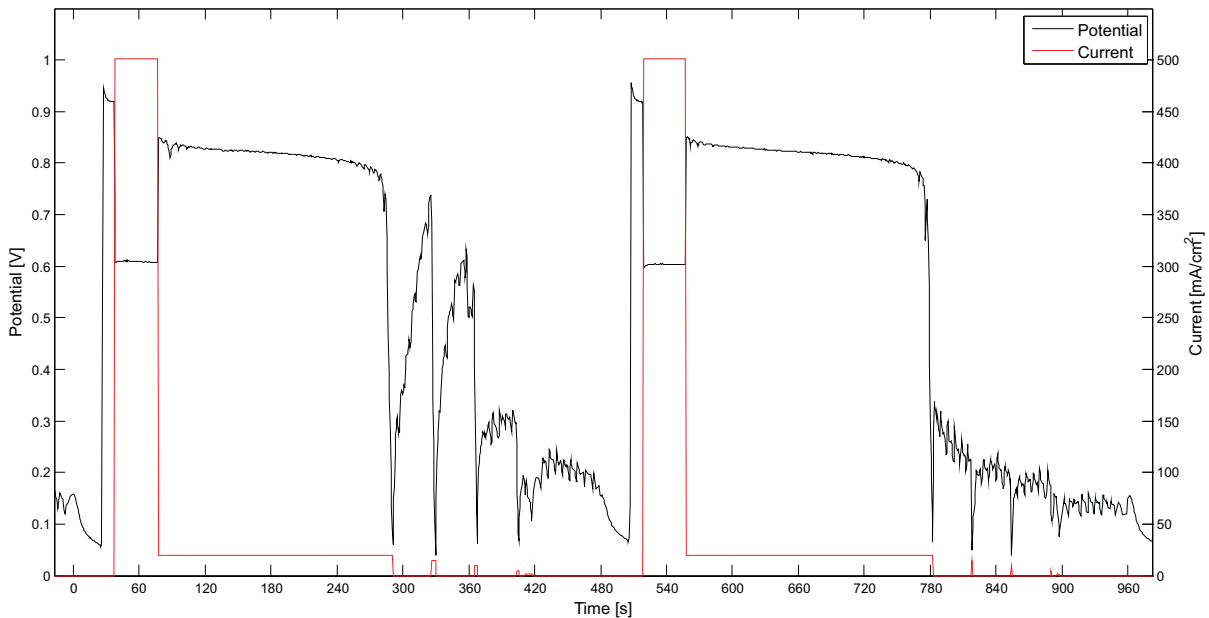


**Figure 2.2:** The current and voltage profiles for two cycles of the recirculation shutdown strategy.

## 2.2 Laboratory Equipment

During operation of a fuel cell, it is important to control different parameters of the cell itself as well as the supplied gases. The cell and gas pipes need to be kept at certain temperatures and the gases have to be hot and humidified. The temperature control is important for the performance of the fuel cell during operation and to prevent formation of water droplets

in the gas pipes. During the test, the pipes and the cell compartment were heated and the gas and cell temperatures were measured by K-type thermocouples, the temperature control was performed by an Eurotherm thermostat. The anode and cathode gases were humidified with bubble humidifiers filled with milli-Q water, which is purified and deionised water.

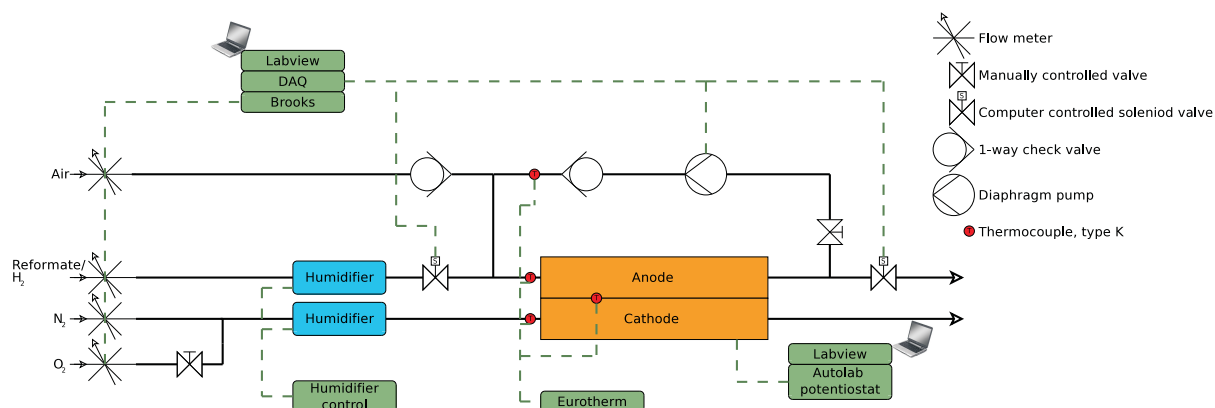


**Figure 2.3:** Schematic of the experimental setup. The dashed lines represent the electrical wires, and the solid lines illustrates the gas pipes.

The gas flows were controlled by solenoid flow meters which were controlled individually via LabVIEW. The same LabVIEW instrument also controlled two solenoid valves and a diaphragm pump, as seen in the schematic in figure 2.3. The signals from LabVIEW to the flow meters, valves and the pump were actuated by two NI USB-6008 DAQs. The solenoid valve placed at the anode inlet prevented leakage of hydrogen from the humidifier and pipes into the fuel cell during purge or recirculation. The solenoid valve at the anode outlet prevented air from diffusing into the anode via the exhaust pipe during recirculation. Two 1-way valves were used to prevent a back flow of gas into the pump, and the air flow meter respectively. The voltage and current operations were performed with an Autolab potentiostat connected to a LabVIEW instrument designed to collect measured data and to run a pre-designed procedure, where the different current and/or voltage control algorithms were programmed. The cyclic voltammetry, impedance spectroscopy, hydrogen crossover and polarization curve measurements were performed with a Zahner IM6 potentiostat.

## 2.3 Performed Analysis Methods

To measure the performance loss during the cycling, a load of  $0.5 \text{ A/cm}^2$  was applied for 40 s in each cycle, and the potential during this load was apprehended. All the *in situ* measurement methods described below were performed before and after the start/stop cycles, in order to analyse the impact of the strategy on the fuel cell. A list of the used parameters in the different methods are presented in table 2.3. The anode was used as the reference electrode in all of the performed measurements.

### Cyclic Voltammetry

Before the cyclic voltammetry was performed, both the anode and cathode was purged with nitrogen, to get rid of residues of oxygen and hydrogen. Then a gas mixture of 5 %  $\text{H}_2$  and 95 % Argon (Ar) was fueled into the anode, while the cathode was supplied with pure nitrogen. The voltage sweep rate was set to  $100 \text{ mV/s}$  in the potential range  $0.50\text{--}1.15 \text{ V}$ .

### Hydrogen Crossover Measurement

During the measurement of hydrogen crossover, pure hydrogen was supplied to the anode and the cathode was supplied with nitrogen. The test was performed by a linear voltage sweep as described in section 1.4.3, from  $110 \text{ mV}$  to  $700 \text{ mV}$ . The current was measured during the sweep, and the crossover current was calculated as a mean of all the measured currents when the potential was higher than  $300 \text{ mV}$ .

### Polarization Curves and Impedance Spectroscopy

The polarization curves were performed in a steady state manner, where each current was drawn in about 20 minutes, which was the time it took for the potential to stabilise, and the impedance measurement to be performed at the specified current. A cut-off limit of  $0.3 \text{ V}$  was introduced to avoid damaging the fuel cell during the measurement. The polarization curves and the impedance spectroscopy were made once for each of the different

fuel/oxidant mixtures  $\text{H}_2/\text{O}_2$ ,  $\text{H}_2/\text{Air}$  and Reformate/Air respectively. The drawn current densities are presented in table 2.3. The flow rate on the cathode side was chosen to be kept constant at 270 ml/min, which implies that the stoichiometry varied between the different amounts of oxygen in the gas mixture. The decision to keep the flow constant was based on that the amount of water should be constant. A changing flow rate would effect both the infusion and outflow of water. The constant parameter on the anode was the stoichiometry, while the flow changed between using hydrogen or reformate as fuel. The stoichiometry on the anode was chosen to be 1.2 to avoid fuel shortages to be a limiting factor. The water content on the anode is not as important as on the cathode, making it more important to keep the stoichiometry constant at the anode side.

### Partial Pressure Sweep

This method was performed as a steady state method, and not as a partial pressure sweep, at the cathode. The different partial pressures of  $\text{O}_2$  and  $\text{N}_2$  were kept constant for about 20 minutes to allow the potential to stabilise, and to perform an impedance measurement at each partial pressure. The current was kept at  $0.5 \text{ A/cm}^2$  and hydrogen was fueled into the anode side during the whole sweep. The flow rate on the cathode was set to 270 ml/min and was kept constant, while the stoichiometry changed with the partial pressure, since the ratio of  $\text{O}_2$  is reduced. The reason for having a constant flow is to keep the amount of water constant on the cathode. The flow rate at the anode was 62.8 ml/min, which implies a stoichiometry of 1.2 at the anode.

**Table 2.3:** Parameters for the different analysis methods performed before and after the cycles.

<b>Cyclic voltammetry</b>	
Anode gas	5 % H <sub>2</sub> 95 % Ar
Anode flow rate	30.2 ml/min
Cathode gas	N <sub>2</sub>
Cathode flow rate	60.0 ml/min
Potential scan range	0.50–1.15 V
Potential scan rate	100 mV/s
<b>Hydrogen crossover measurement</b>	
Anode gas	H <sub>2</sub>
Anode flow rate	30.2 ml/min
Cathode gas	N <sub>2</sub>
Cathode flow rate	60.0 ml/min
Scan range	110–700 mV
Scan rate	0.5 mV/s
<b>Polarization curves and Impedance spectroscopy</b>	
Current densities	0, 1.4, 7.1, 14, 71, 140, 290, 430 ... ... 570, 710, 860, 1000 mA/cm <sup>2</sup>
Anode gas	H <sub>2</sub> or Reformate
Anode flow rate	Varied for each fuel
Anode stoichiometry	1.2
Cathode gas	O <sub>2</sub> or Air
Cathode flow rate	270 ml/min
Cathode stoichiometry	Varied for each oxidant
<b>Partial pressure sweep</b>	
Current density	0.5 A/cm <sup>2</sup>
Anode gas	H <sub>2</sub>
Anode flow rate	62.8 ml/min
Anode stoichiometry	1.2
Percentage of O <sub>2</sub> on cathode	100, 68.4, 36.8, 30, 21, 15, 10
Cathode flow rate	270 ml/min
Cathode stoichiometry	Varied for each partial pressure of O <sub>2</sub>

# Chapter 3

## Results and Discussion

This chapter contains the results from the performed measurements. The OCV and voltage response at  $0.5 \text{ A/cm}^2$  have been measured during the entire start/stop cycling, while the remaining analysis methods were performed before and after 1100 cycles of each strategy. The results will also be discussed to assess the impact the strategies had on the fuel cell performance and characteristics.

### 3.1 Start-up Strategy

The fuel cell was exposed to 1100 cycles of the developed start-up strategy. The details of the strategy are explained thoroughly in section 2.1.1, with corresponding current and potential profiles for two typical cycles in figure 2.1.

The OCV and potential response at  $0.5 \text{ A/cm}^2$  were measured for each cycle and the results are presented in figure 3.1.

After the 1100 cycles the OCV was essentially unchanged. A small linear reduction can be distinguished after the first couple of cycles. The strategy results in an OCV degradation at  $9.9 \mu\text{V/cycle}$ . The fact that the OCV is very stable is an indication of that the strategy has no impact on the internal current or hydrogen crossover parameters, especially the membrane thickness.

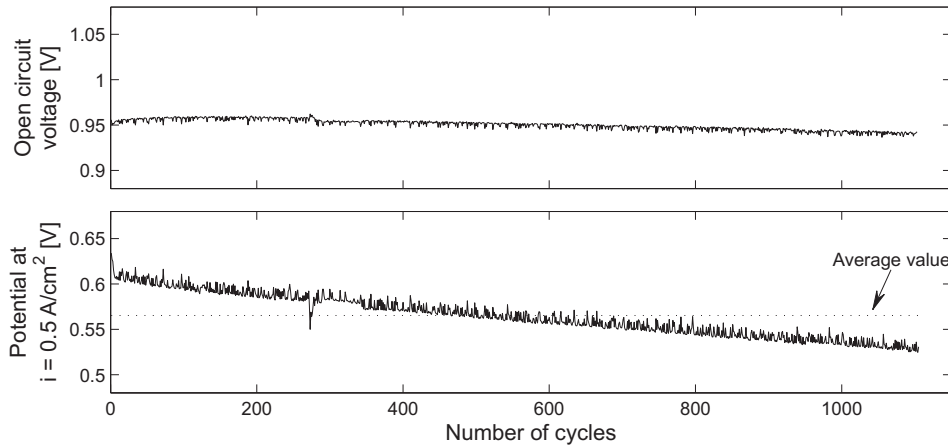


**Figure 3.1:** *The result of the OCV (top) and performance at  $0.5 \text{ A/cm}^2$  (bottom) measurements, at each cycle in the start-up strategy. The OCV is very stable during the whole cycling period, while the potential response at  $0.5 \text{ A/cm}^2$  is reduced by about  $69.7 \mu\text{V/cycle}$ . The average potential response is marked as the dotted line.*

The strategy does however reduce the performance of the fuel cell. When the fuel cell is operated at  $0.5 \text{ A/cm}^2$ , the corresponding potential is reduced by  $69.7 \mu\text{V/cycle}$ . The degradation follows a relatively linear trend since the mean value is crossed after about half of the performed cycles. The normal behavior of a performance reduction of this kind, is that it is slightly faster the first cycles, due to that the not perfectly structured Pt-particles degrade faster. When these particles have disappeared the degradation follows a linear trend. A potential loss of  $69.7 \mu\text{V/cycle}$  or a total reduction of  $12.7\%$  is too large to be accepted in a real application. A summary of the degradation in numbers is presented in table 3.1 in section 3.3.

The first five cycles have a higher potential response at  $0.5 \text{ A/cm}^2$ , as shown in figure 3.1. This is due to that the initial analysis methods were performed with pure hydrogen as fuel, which left remaining hydrogen in the anode humidifier and caused a higher portion of hydrogen in the reformate mixture during these cycles. The drop after 273 cycles is not significant, as it occurred after a restart of the cycling procedure. This event had to be performed, since the water in the humidifiers had to be refilled, the computer was also restarted during this time. The fuel cell anode compartment was purged with dry air before starting the measurement and cycling, which means that the membrane was dried out, making its proton conducting

ability reduced. After some cycles the membrane was humidified again and the performance returned to expected values.

## 3.2 Shutdown Strategy

The recirculation strategy for shutdown was performed for 1100 cycles, as described in section 2.1.2. The potential and current profiles for two cycles are illustrated in figure 2.2.

After 1100 cycles the OCV of the fuel cell is almost unchanged, at about 0.9–0.94 V, as can be seen in figure 3.2. If there was a loss in OCV, it would have been an indication of increased fuel crossover or internal currents. The overall change in OCV is actually an increase of  $39.3 \mu\text{V}/\text{cycle}$  or 4.8%, and would imply that the fuel crossover has been reduced.

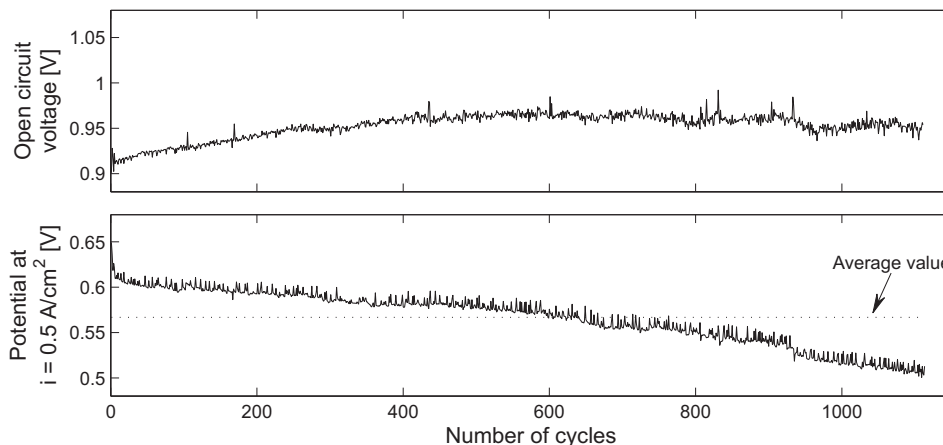


**Figure 3.2:** Measured OCV (top) and performance at  $0.5 \text{ A}/\text{cm}^2$  (bottom) during the recirculation strategy. The OCV is slightly affected by the strategy, the potential response at  $0.5 \text{ A}/\text{cm}^2$  is however reduced by a mean value at about  $92.5 \mu\text{V}/\text{cycle}$ . The dotted line marks the average potential response.

There is however a decrease in the potential when applying a current of  $0.5 \text{ A}/\text{cm}^2$ . The average decrease is  $92.5 \mu\text{V}/\text{cycle}$  or 16.7%, which is relatively severe. The decrease is however not entirely linear. The average value is crossed after 650 cycles, which implies that the degradation is accelerated at high cycles. This accelerated behavior of the fuel cell degradation, can be related to mass transport losses (Jo et al., 2010). A summary of the degradation in numbers can be found in table 3.1 in section 3.3. After

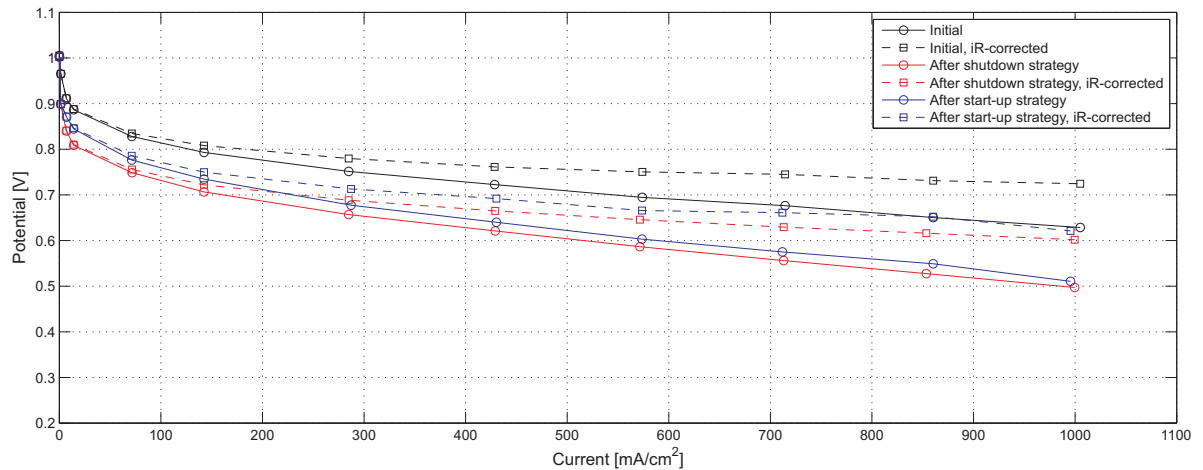
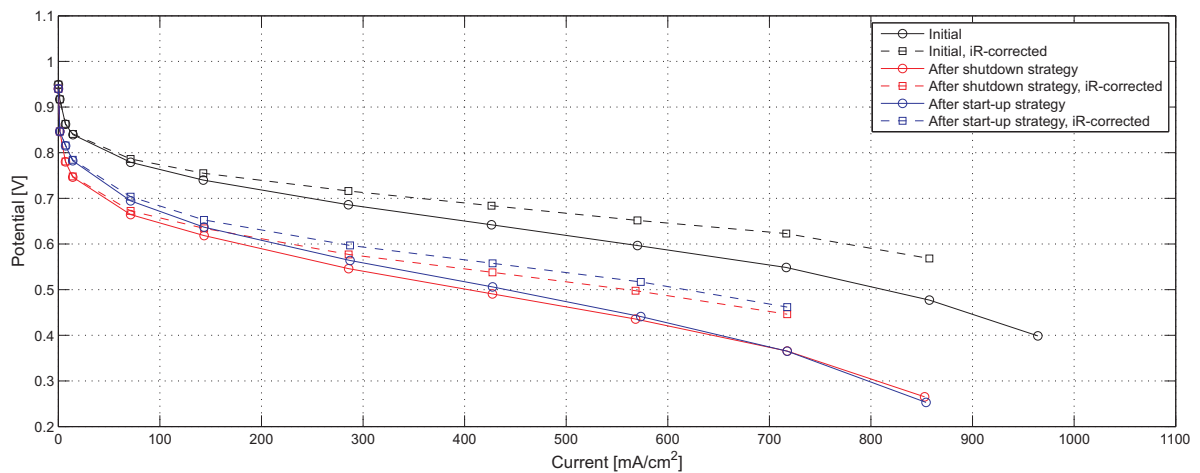
935 cycles, the computer controlling the fuel cell crashed and the fuel cell was operating at OCV without any supply of gases for about six hours. This is the reason for the rapid drop. The potential does however recover and the decrease after this drop is quite linear, thereby the final result might not be affected by this event. The average value is however decreased by the drop, which in turn leads to that the value would have been crossed earlier, and that the performance loss was more linear during the cycling as expected. The drop is also an indication of that operation at OCV for a long time period is not good for a fuel cell. The membrane was also dried out during this time, since there was no supply of humidified gases. The recovering effect of the potential can be assigned to the more humidified membrane during the first of the remaining cycles.

### 3.3 Analysis of the Degradation

This section contains all the measurements performed at an initial stage and after the 1100 cycles were completed for both the start-up and shutdown strategy. Table 3.1 is a summary of the discussed degradation effects.

The polarization curves in figure 3.3(a) is the result of measurements performed with  $H_2$  as fuel and  $O_2$  as oxidant. The solid lines are uncorrected values before and after the cycles, which show a distinct performance degradation after the cycles for both strategies, with a slightly larger degradation for the shutdown strategy. The potential loss increases slightly as the current increases, which indicates mass transport limitations. By using pure  $H_2$  and  $O_2$  the gas transport losses are minimised, thus the mass transport losses originate from a worsened transport of produced water and to a reduced electrochemically active platinum surface area. The dashed lines in figure 3.3(a) are the polarization curves for  $iR$ -corrected cell potentials. The distance between the non-corrected and the corrected curves are about the same before and after the cycles, which is a sign of an almost unchanged ohmic resistance in the fuel cell. The  $iR$ -correction is however slightly larger for the start-up strategy.

The polarization curves in figure 3.3(b) are curves for both non-corrected and  $iR$ -corrected potentials for a measurement performed with reformat

(a)  $\text{H}_2/\text{O}_2$  supplied fuel cell.

(b) Reformate/Air supplied fuel cell.

**Figure 3.3:** Polarization curves of initial measurement and after 1100 cycles of each strategy. The dashed lines are  $iR$ -corrected values of the potential.

as anode gas and air as cathode gas. The polarization curves indicate increased mass transport losses, via the augmented potential drop at high current densities for the measurements performed after the cycles, compared to the initial measurement. The strategies thus damage the porous surroundings of the platinum particles, making the gas pathways narrower and fewer. The produced water transport is also affected by the cycling. There can also be an agglomeration, diffusion and/or coarsening of the platinum catalyst particles during the strategies, that causes the mass transport losses because of a reduced active platinum surface area. The potential loss due to mass transport is larger for the start-up strategy than the shutdown strategy.

To get further information from the polarization curves a Tafel plot was made at current densities lower than  $100 \text{ mA/cm}^2$ . By approximating the measured data in a non-linear least square fit manner, and plot the activity loss against the logarithm of the current density, the Tafel plot in figure 3.4 was apprehended. As described in section 1.4.1 the slope of the linear region corresponds to the material parameter  $A$  and the point where the dashed line crosses the x-axis correspond to the ORR exchange current  $i_0$ . The slopes are increased when both strategies are performed. The slopes are also similar between the two curves corresponding to the measurements after 1100 cycles, indicating that usage of the fuel cell has a similar effect on this parameter. The ORR exchange current has however decreased more for the shutdown strategy, which could imply larger effects on the platinum catalyst supports, leading to reduced ECSA.

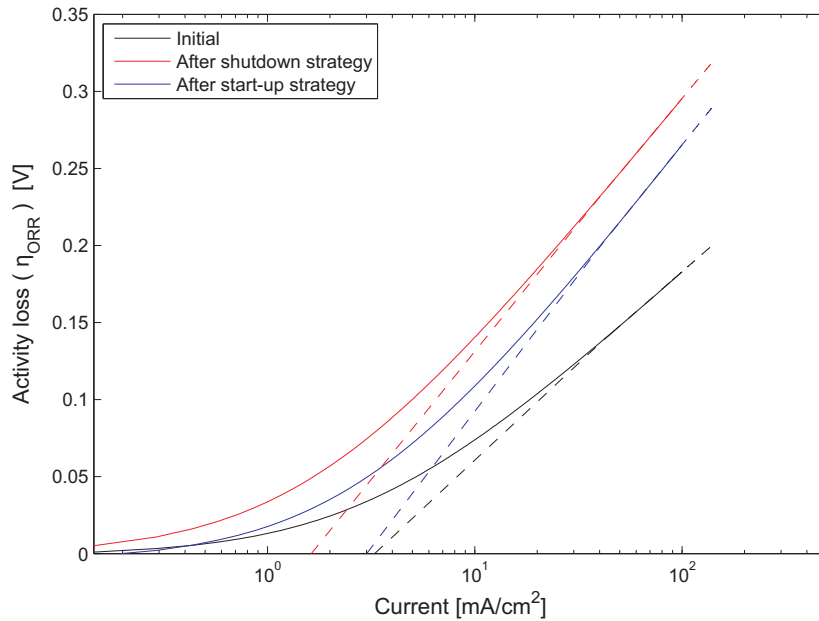


**Figure 3.4:** Tafel plot of the measurements performed at an initial stage and after the two strategies. The data comes from a non-linear least square approximation of the polarization curves, at low current densities ( $i < 100 \text{ mA/cm}^2$ ).

Figure 3.5 shows the increase of the activity losses, ohmic losses and mass transport losses, compared to the initial values. The comparison is made on a Reformate/Air fueled fuel cell operated at a current density of  $860 \text{ mA/cm}^2$ , which is high enough to cause mass transport losses. The red line indicates that the ohmic losses stay almost unaffected by the cycling. The activity losses cause the highest potential loss, but it is not as affected by the cy-

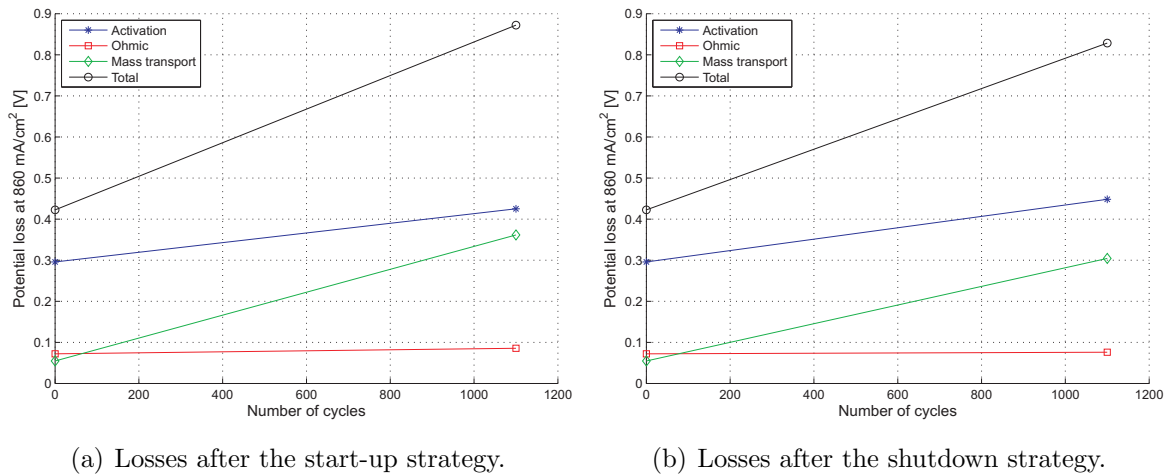


**Figure 3.5:** Comparison of the increase of each loss on the polarization curve. The losses are taken from the measurement with Reformate/Air at  $860 \text{ mA/cm}^2$ .

cling as the mass transport losses. The largest degradation appears in the mass transport for the start-up strategy, which has increased almost six times compared to the initial value.

The change in mass transport properties can also be deduced from the partial pressure sweep in figure 3.6. When there is pure  $\text{O}_2$  on the cathode side, is it feasible to assume that the potential loss is due to other events than mass transport. While the reduction of  $\text{O}_2$  in the cathode gas is progressing, the difference between the two curves is increasing, which is a verification of that a degradation due to mass transport is present. In contrast to the result from the polarization curves in figure 3.3(b), the start-up strategy shows a smaller mass transport loss compared to the shutdown strategy. The difference between the two methods to measure the mass transport loss, is that the current is constant and the gas stoichiometry is varied during the partial pressure sweeps, and vice versa for the polarization curve measurement. This fact makes it assumable that the mass transport losses for the start-up strategy is due to resistive and/or conductive effects. The mass transport losses for the shutdown strategy can however be more related to gas and produced water management.

The results of the performed impedance spectroscopies at  $i = 14 \text{ mA/cm}^2$  are shown in the Nyquist plot in figure 3.7. This current density was chosen because it is low enough to ensure that mass transport losses due to

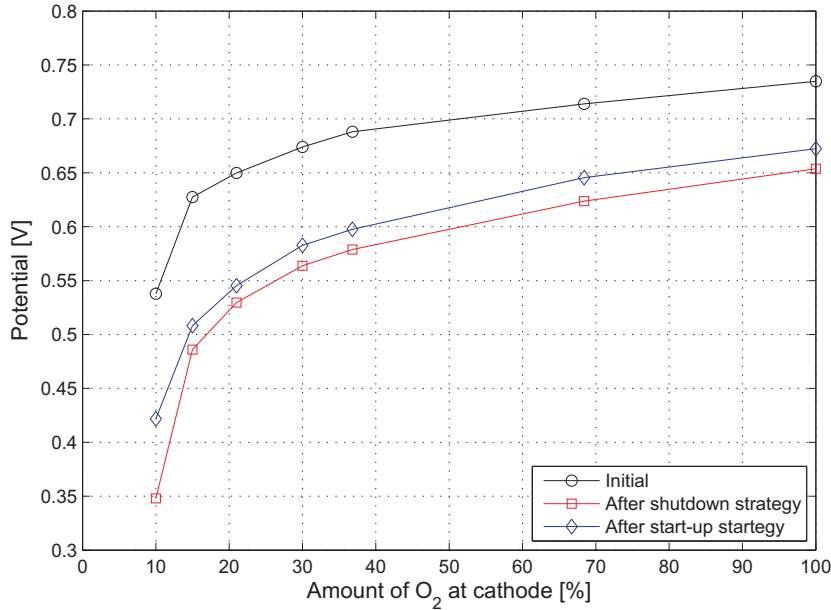


**Figure 3.6:** Results from the partial pressure sweep measurements before and after 1100 cycles of the strategies. An increased loss due to mass transport can be seen by analysing the increased distance between the curves, during the reduced oxygen amount.

gas and product water transport can be neglected, making the changes depend on degradation of the catalytic properties. The spectroscopy is performed for each of the three fuel/oxidant combinations used in this thesis, which are H<sub>2</sub>/O<sub>2</sub>, H<sub>2</sub>/Air and Reformate/Air. The enlarged diameters on the impedance semicircles indicate that the charge transfer resistances increase in the cathode electrode during the cycles for both strategies. The effect is enlarged when air is used as the cathode gas instead of pure O<sub>2</sub>, which indicates that the gas and produced water transport properties are affected when operating the fuel cell. There is also an enlarged charge transfer resistance when reformate is used as fuel, which can be seen when comparing the changed diameters between the non-solid curves of each strategy. This is on the other hand not affected by the cycling, since the difference between these curves measured with air and H<sub>2</sub> or reformate, after cycling compared to the initial state, is similar. The most interesting result is that the  $R_{ct}$  increase is much larger for the start-up strategy than for the shutdown strategy. The increase is about  $0.8 \Omega\text{cm}^2$  for the start-up strategy, but only  $0.1 \Omega\text{cm}^2$  for the shutdown strategy. This confirms the conclusion drawn from the polarization curves and the partial pres-

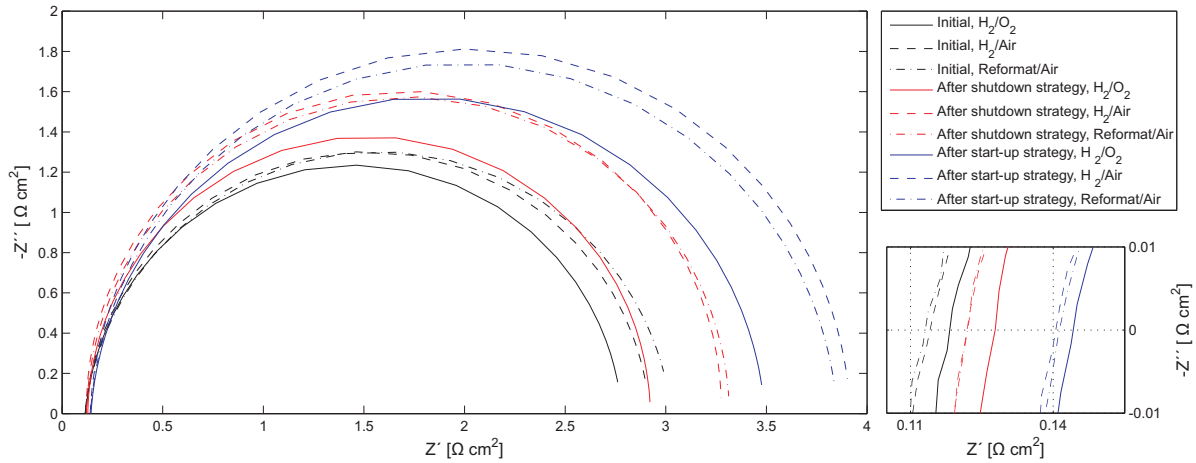


**Figure 3.7:** Impedance spectroscopy performed at  $14 \text{ mA/cm}^2$  before and after the strategies. The diameters increase after 1100 cycles, which corresponds to an increased charge transfer resistances. The two cases with air on the cathode also increases  $R_{ct}$ . The small figure shows an enlargement of the high frequency intercept, which corresponds to  $R_{mem}$ .

sure sweep, that the mass transfer loss after the start-up strategy is more influenced by degradation of the catalytic properties.

The disturbance effect of the double layer capacitance can also be evaluated when comparing the height with the width of each semicircle. As described in section 1.4.4, the height should be equal to half the width if there was no disturbance. This is approximately the case for all the nine curves in figure 3.7, which means that the double layer stay almost purely capacitive even after cycling.

The membrane resistances has been affected during the cycling, as can be seen in the enlarged section of figure 3.7. The membrane resistance is the point where the curves crosses the real axis (x-axis), hence all membrane resistances are between  $0.111\text{--}0.142 \Omega \text{ cm}^2$ . The largest  $R_{mem}$  increase is for the start-up strategy.

The impedance spectroscopy presented in figure 3.8, shows the result of a measurement performed at a current density of  $710 \text{ mA/cm}^2$ , for the three different fuel/oxidant alternatives, at an initial stage and after performing the two cycling strategies. The current density is high in this case, and the change in  $R_{ct}$  will be more related to gas and water transport at the cathode compartment. Figure 3.8 shows a similar  $R_{mem}$  ( $\approx 0.1\text{--}0.15 \Omega \text{ cm}^2$ ) for all

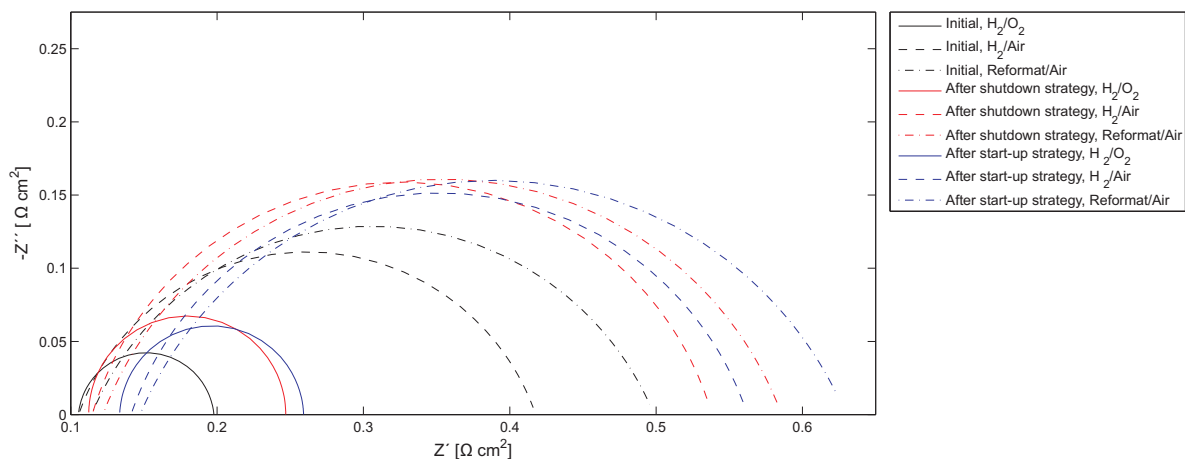


**Figure 3.8:** Impedance spectroscopy performed at  $710 \text{ mA/cm}^2$  before and after the strategies. The increase in diameter is similar for both of the strategies, which means that  $R_{ct}$  is affected similarly of the two strategies, at high current.

of the arcs, which concurs with the results from the impedance spectra at lower current density, presented in figure 3.7. The effect of increased  $R_{ct}$  when using reformat also applies at high current densities. The interesting result in figure 3.8, is that the diameters of the semicircles measured after performing the two strategies are similar, in opposite to the corresponding arcs in figure 3.7. This strengthens the conclusion that degradation of the catalytic properties is responsible for the larger mass transport loss after performing the start-up strategy, compared to the shutdown strategy.

The results from the performed cyclic voltammetry experiments are shown in figure 3.9. Both the start-up and shutdown strategies have decreased the electrochemically active platinum surface area during the 1100 cycles. The integrated area under the hydrogen adsorption peak, as described in section 1.4.2, has decreased by about 81.4% for the start-up strategy and 75.9% for the shutdown strategy, which corresponds to the total ECSA decrease. The decreased ECSA is a clear sign of that the platinum particles have agglomerated, oxidized and/or diffused. Corrosion of the platinum particle supports can be assumed to be responsible for the main part of the reduced ECSA, thereby it is fair to assume that reverse currents have occurred during the cycling of the two strategies and that the resulting high potentials caused carbon corrosion. Between 0.3–0.4 V of the cyclic voltammetry, the curves came closer during operation of the strategies,

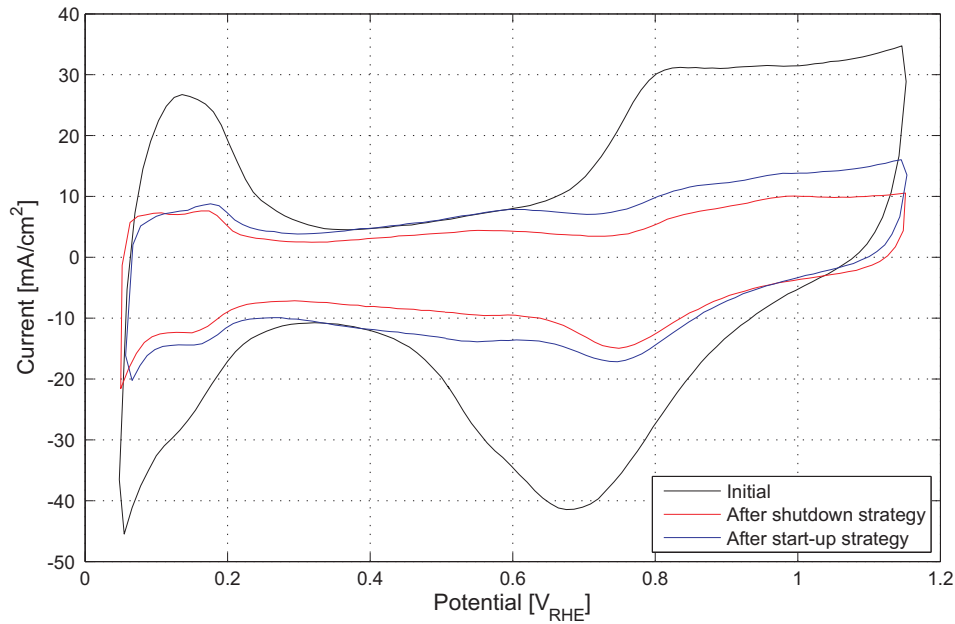


**Figure 3.9:** Result of cyclic voltammetry performed before and after 1100 cycles of the strategies. The active ECSA has reduced by about 81.4 % and 75.9 % during the start-up and shutdown strategy respectively.

which indicates that the double layer capacitance has decreased. The PtO reduction peak at potentials around 0.7 V decreases in intensity and shifts slightly to higher potentials after the 1100 cycles. This event can, according to Seo et al. (2010), depend on larger platinum particles due to sintering.

The hydrogen crossover was measured with a potential sweep method. By calculating the mean value of the currents at potentials above 0.3 V, the crossover currents are estimated. The results of the measurements, presented in figure 3.10, shows that the initial crossover current is higher than the crossover currents measured after performing 1100 cycles of the two strategies. This result is surprising, because the hydrogen crossover is assumed to increase during operation, due to degradation of the membrane, which lead to thinner membranes and formation of pin-holes. The reduced crossover current would indicate that the membrane has become more compact. Another conclusion that can be drawn is that the start-up strategy results in higher crossover current than the shutdown strategy. This might be due to high current peaks for some of the cycles, during the potential control sequence between 30–60 s in the cycle. These current peaks cause elevated temperatures and that might result in pin-hole formation.

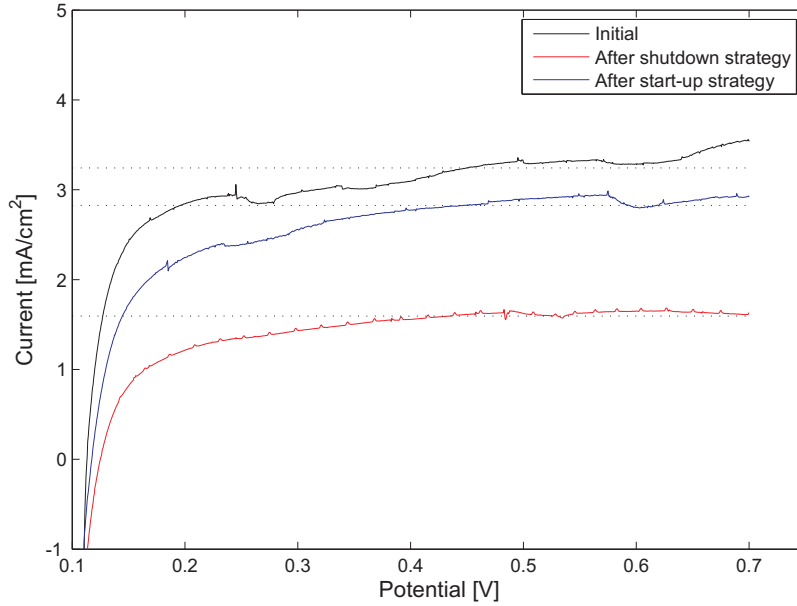


**Figure 3.10:** Results of hydrogen crossover measurements before and after the strategies. The initial crossover current density was estimated to  $3.2 \text{ mA/cm}^2$ . The crossover currents after 1100 cycles were  $2.8 \text{ mA/cm}^2$  and  $1.6 \text{ mA/cm}^2$  for the start-up and shutdown strategy respectively.

**Table 3.1:** Comparison of the discussed degradation parameters. The values from the polarization curve is the same as presented in figure 3.5. The  $R_{ct}$  and  $R_{mem}$  values are from the curves measured with reformate as fuel and air as oxidant. The values in parenthesis is the percental change, compared with the initial values.

	Initial	After start-up strategy	After shutdown strategy	Analysis method
$\eta_{ORR}$ [V]	0.296	0.425 (43.6)	0.488 (51.6)	Polarization curve
$iR_{\Omega}$ [V]	0.072	0.086 (18.6)	0.076 (5.2)	Polarization curve
$\eta_{tx}$ [V]	0.055	0.362 (561)	0.304 (457)	Polarization curve
$i_x$ [ $\text{mA/cm}^2$ ]	3.24	2.82 (-13.0)	1.59 (-50.9)	Hydrogen crossover
$R_{mem}$ [ $\Omega\text{cm}^2$ ]	0.114	0.147 (29.0)	0.122 (6.7)	Impedance spectroscopy
$R_{ct}^{14}$ [ $\Omega\text{cm}^2$ ]	2.92	3.71 (27.3)	2.97 (9.5)	Impedance spectroscopy
$R_{ct}^{710}$ [ $\Omega\text{cm}^2$ ]	0.384	0.482 (25.5)	0.4638 (20.7)	Impedance spectroscopy
ECSA [%]	–	-75.9	-81.4	Cyclic voltammetry
$C_{dl}$ [ $\text{mF/cm}^2$ ]	76.5	68.8 (-10.0)	48.0 (-37.2)	Cyclic voltammetry

## Chapter 4

# Conclusion and Future Work

In a sustainable future the fuel cell technology is an interesting building block. It has high efficiency and is virtually free from green house gas emissions, when fueled with hydrogen. In a future energy sector, it is possible that the hydrogen can work as an energy storage. If solar, wind or water energy is used to produce hydrogen, it can be stored and used efficiently in fuel cells whenever and wherever it is needed. The efficiency, lifetime and cost of the fuel cells are getting closer to the target, but there are still some issues left to solve before fuel cells can be fully commercialized. Protective start-up and shutdown strategies are very important to increase the lifetime of a fuel cell.

Both the tested potential control start-up strategy and the recirculation shutdown strategy were much better than doing nothing at all. Ivity (2010) found that the fuel cell potential was significantly reduced already after 125 cycles, when the cell was started and stopped without any protective strategy at all. The two strategies tested in this paper degraded the fuel cell in a similar manner and the potential loss at  $0.5 \text{ A/cm}^2$  was about the same. The start-up strategy did degrade the ECSA more than the shutdown strategy, which resulted in larger charge transfer resistance, that increased mass transport losses. The degradation of the fuel cell performance was too high, for both strategies, in order to apply them in a real application. A satisfying degradation would be lower than approximately  $10 \mu\text{V}/\text{cycle}$ . Since the degradation was similar for both of the strategies, a possible reason for the degradation could be the instantaneous load of  $0.5 \text{ A/cm}^2$ . A slower change of the load would have been better for the fuel cell.

To further improve the start-up and shutdown protection strategies, tests have to be performed with strategies for both start-up and shutdown applied at the same time. When the start-up and the shutdown strategies are tested separately, it can be the unprotected sequence that causes the most of the degradation. Before applying the strategies in an application, it is also important to run the strategies for more cycles and with a fuel cell stack. The different properties in gas distribution and series connections between the each single cell in the stack would probably change the degradation behavior.

# Bibliography

- Baumgartner, W. R. R. , et al. (2006). ‘Electrocatalytic Corrosion of Carbon Support in PEMFC at Fuel Starvation’. *ECS Transactions* **3**(1):811–825.
- Borup, R. , et al. (2007). ‘Scientific Aspects of Polymer Electrolyte Fuel Cell Durability and Degradation’ **107**(10):3904–3951.
- Carter, R. N. , et al. (2009). *Handbook of Fuel Cells - Fundamentals, Technology and Applications*, vol. 6. John Wiley & Sons, Ltd., 2 edn. Part 2, Chapter 56.
- Darling, R. M. & Meyers, J. P. (2003). ‘Kinetic Model of Platinum Dissolution in PEMFCs’. *Journal of The Electrochemical Society* **150**(11):A1523–A1527.
- de Bruijn, F. , et al. (2008). ‘Review: Durability and Degradation Issues of PEM Fuel Cell Components’. *Fuel Cells* **8**(1):3–22.
- Gasteiger, H. A. , et al. (2008). ‘Catalyst Degradation Mechanisms in PEM and Direct Methanol Fuel Cells’. In S. Kakaç, A. Pramuanjaroenkij, & L. Vasiliev (eds.), *Mini-Micro Fuel Cells*, NATO Science for Peace and Security Series, pp. 225–233. Springer Netherlands.
- Gasteiger, H. A. , et al. (2004). ‘Dependence of PEM fuel cell performance on catalyst loading’. *Journal of Power Sources* **127**(1-2):162 – 171. Eighth Ulmer Electrochemische Tage.
- Ivity, M. (2010). ‘Shutdown strategies for Polymer Electrolyte Membrane Fuel Cell to Minimize Degradation’. Master’s thesis, Chalmers University of Technology.

- Jo, Y. Y. , et al. (2010). ‘Effects of a hydrogen and air supply procedure on the performance degradation of PEMFCs’. *International Journal of Hydrogen Energy* **35**(23):13118 – 13124. Asian Hydrogen Energy Conference 2009.
- Kim, J. H. , et al. (2009). ‘Development of a Durable PEMFC Startup Process by Applying a Dummy Load’. *Journal of The Electrochemical Society* **156**(8):B955–B961.
- Kim, J. H. , et al. (2010a). ‘Effects of Cathode Inlet Relative Humidity on PEMFC Durability during Startup–Shutdown Cycling’. *Journal of The Electrochemical Society* **157**(1):B104–B112.
- Kim, J. H. , et al. (2010b). ‘Effects of Cathode Inlet Relative Humidity on PEMFC Durability during Startup–Shutdown Cycling’. *Journal of The Electrochemical Society* **157**(5):B633–B642.
- Kocha, S. , et al. (2006). ‘Characterization of gas crossover and its implications in PEM fuel cells’. *AIChE Journal* **52**:1916 – 1925.
- Larminie, J. & Dicks, A. (2003). *Fuel cell systems explained*. John Wiley and Sons Ltd, 2 edn.
- Lindström, R. W. , et al. (2010). ‘Active Area Determination of Porous Pt Electrodes Used in Polymer Electrolyte Fuel Cells: Temperature and Humidity Effects’. *Journal of The Electrochemical Society* **157**(12):B1795–B1801.
- Marie, J. , et al. (2009). ‘Highly porous PEM fuel cell cathodes based on low density carbon aerogels as Pt-support: Experimental study of the mass-transport losses’. *Journal of Power Sources* **190**(2):423 – 434.
- Meyers, J. P. & Darling, R. M. (2006). ‘Model of Carbon Corrosion in PEM Fuel Cells’. *Journal of The Electrochemical Society* **153**(8):A1432–A1442.
- Nakamura, S. , et al. (2009). ‘The diffusion overpotential increase and appearance of overlapping arcs on the Nyquist plots in the low humidity temperature test conditions of polymer electrolyte fuel cell’. *Journal of Power Sources* **186**(2):278 – 285.

- Ofstad, A. , et al. (2008). ‘Carbon Corrosion of a PEMFC During Shut-down/Start-up when Using an Air Purge Procedure’. *ECS Transactions* **16**(2):1301–1311.
- Perry, M. L. , et al. (2006). ‘Systems Strategies to Mitigate Carbon Corrosion in Fuel Cells’. *ECS Transactions* **3**(1):783–795.
- Reiser, C. A. , et al. (2005). ‘A Reverse-Current Decay Mechanism for Fuel Cells’. *Electrochemical and Solid-State Letters* **8**(6):A273–A276.
- Seo, D. , et al. (2010). ‘Physical degradation of MEA in PEM fuel cell by on/off operation under nitrogen atmosphere’. *Korean Journal of Chemical Engineering* **27**:104–109.
- Shen, Q. , et al. (2009). ‘Study on the processes of start-up and shut-down in proton exchange membrane fuel cells’. *Journal of Power Sources* **189**(2):1114 – 1119.
- U.S. Department of Energy, (2009). ‘Hydrogen and Fuel Cell Activities, Progress and Plans: Report to Congress’. 19–20.
- Young, A. P. , et al. (2009). ‘Characterizing the Structural Degradation in a PEMFC Cathode Catalyst Layer: Carbon Corrosion’. *Journal of The Electrochemical Society* **156**(8):B913–B922.
- Young, A. P. , et al. (2010). ‘Ionomer Degradation in Polymer Electrolyte Membrane Fuel Cells’. *Journal of The Electrochemical Society* **157**(3):B425–B436.
- Yu, P. T. , et al. (2009). ‘Carbon-Support Requirements for Highly Durable Fuel Cell Operation’. In F. N. Büchi, M. Inaba, & T. J. Schmidt (eds.), *Polymer Electrolyte Fuel Cell Durability*, pp. 29–53. Springer New York.
- Yuan, X.-Z. , et al. (2010). *Electrochemical Impedance Spectroscopy in PEM Fuel Cells Fundamentals and Applications*. Springer London.